The Thesis Committee for Edward Park
Certifies that this is the approved version of the following thesis:

Temporal and Spatial Analysis of Suspended Sediment Distribution in the Amazon River using Satellite Imagery

APPROVED BY
SUPERVISING COMMITTEE:

Supervisor:

Edgardo M. Latrubesse

Eugenio Y. Arima

Kelley A. Crews

Temporal and Spatial Analysis of Suspended Sediment Distribution in the Amazon River using Satellite Imagery

by

Edward Park. B.A.

Thesis

Presented to the Faculty of the Graduate School of

The University of Texas at Austin

in Partial Fulfillment

of the Requirements

for the Degree of

Master of Arts

The University of Texas at Austin

May 2013

Dedication

Dedicated to my family: Yaelim, Dongsun, Nohyoung, Young, Hye-yeon, Tae-young, Ji-in and grandparents. Thank you so much for your trust, support and love.

Abstract

Temporal and Spatial Analysis of Suspended Sediment Distribution in the Amazon River using Satellite Imagery

Edward Park, M.A.

The University of Texas at Austin, 2013

Supervisor: Edgardo M. Latrubesse

Patterns of surface sediment concentration distribution in rivers are significant for understanding the broad ranges of fluvial environmental systems. In the case of the Amazon Basin, the complexity in the sediment pattern distribution is affected by the anabranching channel pattern of the Amazon River, the input by tributaries (some of which are among the largest rivers on earth) and the existence of huge and complex floodplains. Until recently, the assessment of sediment fluxes has been concentrated on hydro-sedimentological techniques in the Amazon Basin; however, efforts on characterizing the patterns of sediment transport have been neglected.

This study aims to improve the understanding of the pattern of sediment distributions over a large scale in the Amazon River by estimating surface sediment concentration with remote sensing techniques. Field acquired surface sediment concentration values were supplied from three gauging stations representing the

upstream, midstream and downstream sections of the Amazon River from 2000 to 2010 and calibrated with MODIS surface reflectance products (N=207, 232, 313, respectively). Empirical models were derived with robust causalities ($0.63<R^2<0.92$) between field surface sediment concentration and surface reflectance from each station; however, sensitivity of reflectance around each stations were shown to be significantly affected by the local hydrological behaviors, leaving implications on analysis of the geomorphic characteristics affecting these associations. Overall, the capability of the remote sensing-based platform introduced in this study is successfully demonstrated by capturing the spatial and temporal variability of surface sediments in the Amazon River Basin, which is the largest and the most complex river system on earth.

Table of Contents

List of Tables

List of Figures

List of Equations

Chapter 1: Introduction

1.1 BACKGROUND

Understanding the patterns of sediment transport, erosion and deposition is a crucial factor in studying large rivers, because sediments play a major role in the geomorphic evolution of the channel and its floodplain systems and biogeochemical cycle (Latrubesse et al, 2005; Latrubesse, 2008; Mertes et al., 2007). In addition, changes in sediment quantity and quality in rivers can have significant impacts on a broad range on the environmental systems. Therefore, mapping aggradational landforms in rivers has been a focus for the river scientists across the disciplines concerning the fluvial environments. However, the assessment of sediment fluxes has been concentrated on hydro-sedimentological techniques and, until recently, the identification of patterns of sediment transport of suspended sediments was almost unknown.

For large rivers such as the Amazon River, sediments in suspension are predominantly composed of sediment particles sized of silt and clay (i.e. wash loads). The concentrations (mg/l) of total suspended particles usually show very small differences with that of the water surface, though their differences vary locally and seasonally (Filizola et al., 2011). Optical properties of suspended sediments are normally reflected from organic acids absorbed in the water column (Witte et al, 1981), which makes the analysis of spectral characteristics of the surface suspended sediments reasonable. Due to this optical property of surface sediments, nonlinear signals from sensors mounted on satellites shows robust association with color of surface water

(Albanakis, 1990; Bhargava et al., 1991; Baker et al., 1984; Curran et al., 1988). Hence, examination of surface water quality with remote sensing techniques has been a major focus for remote sensing scientists since the first earth observation satellites were launched in the early 1970s (Mertes et al., 2007).

1.2 RELATED WORKS

Conventional methods

Traditionally, numerous studies were presented to understand suspended sedimentary processes in the Amazon Basin with different objectives. Supported from various governmental agencies, projects such as Carbon in the Amazon River Experiment (CAMREX) and Geodynamical, hydrological and biogeochemical control of erosion/alteration and material transport in the Amazon basin (HYBAM) provided various types of hydrologic data at different gauging stations across the Amazon basin, including water level, discharge, ADCP measurements, sediments, and physio-chemical, geochemical properties. Though these efforts have contributed to improvements in regional scale studies, point-based measurements in a river cross section show limitations in examining the spatial distribution of suspended sediments and their changes throughout time. Works done by Dunne et al. (1996) and Mertes et al. (1998) have led to methodologies developed to calculate sediment budgets in the Amazon River mainstream (including Solimoes and Amazon River), which give a general framework on patterns of suspended sedimentary processes along the river and their exchange between floodplains at a continental scale. Their works have provided useful insights on sedimentary

processes in the Amazon Basin; yet, significant studies have not been done on understanding the spatial distribution at local scales and time-series analysis of suspended sediments only recently became possible with the availability of higher temporal resolution remotely sensed imagery.

Remote sensing application

After the Earth Observation Satellites (EOS) were launched and remote sensing images became widely available, river scientists started to link surface sediment concentration rates to the surface reflectance recorded in remote sensing data and, in particular, the strong responses within the visible light portion of the electromagnetic spectrum as a function of sediment concentration at water surface enabled retrieval of absolute surface sediment load from space. Starting with the Landsat program in the 1980s, this method has been proven to be relevant by a number of different remote sensing instruments such as SeaWiFS, SPOT and MODIS with high accuracies and root mean square errors (RMSE) ranging from 10 to 20 mg/l per pixel. Needless to say, along with the rapidly evolving capabilities of remote sensing instruments, more frequent and accurate estimations of surface sediments in both smaller and larger spatial scales became possible.

Remote sensing approaches in estimating surface sediment concentrations have been applied to various regions across the earth, including the Mississippi River and its delta (Miller et al., 1995, 2004), the Gulf of Maine (Stumpf et al., 1992), in Puerto Rico (Rodríguez-Guzmán et al., 2009), the Mediterranean Sea (Tassan, 1994), China (Bi et al., 2011; Li et al., 1998; Wang et al., 2010; Zhang et al., 2010), and Korea (Min et al., 2012).

In the Amazon basin, in particular, several works have been conducted with different objectives and methods (Mertes et al., 1993; Martinez et al., 2009; Kilham et al., 2011; Villar et al., 2012). In general, two different calibration methods have been applied in order to estimate surface sediment concentration through remote sensing techniques in the Amazon basin: a) experiment-based (Mertes et al., 1993; Kilham et al., 2011); and b) observation-based (Martinez et al.2003, 2009; Villar et al., 2012). Experimental methods use spectroradiometers in a lab configuration to extract spectral end-members, based on which fraction-images depicting different sediment concentrations can be derived. Experimental studies established a fine foundation for the observational method by detecting direct causality between the variables of interest (i.e. proportion of reflected light according to a given sediment concentration).

Both the experimental and observational calibration methods have pros and cons. Due to the unsystematic gauging conducted from the 1970, and the disagreeing time line with remote sensing systems with moderate temporal resolution (prior to the launch of MODIS in 1999), researchers experienced a shortage in available data and developed methods that could be relied on with only a few observations. For example, in retrieving end-members, both Mertes (1993) and Kilham (2011) used data from the CAMREX field campaigns conducted from 1982 to 1991. Lab experimentation is efficient in detecting the causality between sediment concentration and reflectance; however, it is difficult to understand the variability of associations depending on seasons and regions, since this method provides a single brightness value for each end-member. The observational calibration method, which uses a large number of samples acquired at different temporal

and spatial scales, allows for a wide range of responses and associated patterns. Using this observational method, Martinez (2009) quantified a sediment budget of the Amazon River and Villar (2012) examined the seasonal variability in surface reflectance in the Madeira River, also in the Amazon Basin. In this study, the observational method is implemented to verify the spatial and temporal variability of surface sediment concentration with an unprecedentedly large sampling from three different gauge stations:Tabatinga, Manacapuru and Obidos.

1.3 MOTIVATION OF THE STUDY

Although several different methods have been proposed to estimate surface sediment rates in the Amazon River Basin using remote sensing data from different studies, their objectives were different. Martinez et al., (2009) were interested in sediments transport in single site (i.e. sediment flux in Obidos), while Villar et al. (2012) focused on retrieving a calibration model from different sites in an Amazonian tributary (i.e. Madeira River). Mertes et al., (1993) estimated surface sediments in the Amazon Basin using Landsat in order to examine channel-floodplain interactions. However, study for the comprehensive understanding of the dynamic patterns of surface sediment distribution over a larger area (including floodplains and confluences) in Amazon River's mainstream (e.g., the reach from Tabatinga to Obidos, Fig. 1) using remote sensing has not been performed. Monitoring and analyzing different surface sediment patterns through time enables not only the examination of sediment transport along the multi-channel system (i.e. anabranching channels, Latrubesse et al., 2008), but also the

investigation of the surface sediment interaction with complex floodplains (Latrubesse, 2012) and impacts of tributaries (e.g. Negro, Madeira, Tapajos River, etc). Moreover, previous studies performed using lab spectrometers from surface sediment concentration end-members obtained from specific sites were not designed to capture the temporal (seasonal) variations of surface sediment properties, which influence its reflectance. Other similar studies using multi-temporal surface sediment data performed in one specific region were not designed to capture the spatial dependency of surface sediment properties, which also determine its reflectance. Therefore, there are specific needs to both comprehensively understand the spatial and temporal distribution pattern of surface sediment concentration and examine variations of models from different time and space in the Amazon River, which is investigated throughout this study.

1.4 OBJECTIVES

This study mainly aims to build a platform that will allow the estimation of surface sediment distribution patterns in a multi-temporal scale using remote sensing data in a large river basin. With this platform, I expect to address the larger goals of the overall geomorphologic project: understanding the spatial and temporal patterns of distribution of surface sediment in mega river systems. As mentioned in the previous section (1.3), interpretation about surface sediment's spatial and temporal distributions from geomorphologic and environmental perspectives has been extremely lacking in the literature, which is key in understanding morpho-dynamics in large fluvial systems such as Amazon River. Therefore, in this study, I will demonstrate the capabilities of my

platform to mainly understand: a) sediments' channel-floodplain interactions in higher resolutions; b) variability of surface sediment distribution in different branches along main channel; c) impacts of both large and small tributaries along the main channel. A secondary objective of this study is to d) explore valid associations between surface sediment concentration and reflectance in different time and space within Amazon River mainstream. Analyzing the models retrieved from different time and space will provide guidance in understanding the geomorphologic and environmental properties affecting the associations of surface sediment concentration and reflectance in the complex fluvial systems.

Chapter 2: Materials and Methods

2.1 STUDY AREA

Amazon River system

The Amazon River Basin, the largest river basin in the world, covers about 5% of the land on the earth, amounting to approximately six million square kilometers (Filizola et al., 2005). Given this largest size in area, the Amazon Basin's mean annual discharge runs up to nearly 210000 m^3/s, contributing approximately 20% of the annual global fresh water discharge to the ocean (6,300 km^3). The Amazon River[1] begins in the Andean Mountains, which occupy approximately 12% of the area of the Amazon Basin, and travels more than 3,000 km to reach the Atlantic Ocean (Fig. 1). Considering its enormous scale, it is not surprising that among the 10 largest rivers in terms of water discharge in the world[2], four mega-rivers flow through the Amazon Basin (Amazon, Madeira, Negro, and Japura River), and 24 of the 34 largest tropical rivers are in the Amazon Basin or are related to the Amazon Rainforest (Latrubesse, 2008, 2012; Latrubesse et al., 2005). These mega rivers present complex multi-channel and floodplain systems, which follow the anabranching system (Latrubesse et al., 2008).

As the largest river in terms of water discharge on the planet, the Amazon River has one of the largest sediment yields in the world with approximately 1,240 million tons

[1] When the River enters Brazil, it is known as Solimões River and when it meets the confluence with Negro River, it is known as Amazon River; however, in this study mainstream of whole Amazon River system is referred as Amazon River for convenience purpose.

[2] Amazon, Congo, Orinoco, Yang Tse, Madeira, Negro, Brahamaputra, Japura, Parana, Mississippi River (in order of annual discharge).

per year (Mertes et al., 1996). Over 90% out of this tremendous amount of transported sediment along the Amazon River is the result of local erosional processes originating in Andean tributaries (Latrubesse et al., 2005). The two major contributing tributaries to total sediment yield are the Solimões River and the Madeira River. The Solimões River, which drains the Peruvian Andes and crosses a wide alluvial plain, has a rich suspended load (approximately 400 million tons mean suspended sediment, Filizola et al., 2009). The Madeira River, which drains the Bolivian, Peruvian Andes and crosses the Brazilian Shield, is estimated to take up around 50% of total suspended load transported by Amazon River to the Atlantic Ocean (projected total suspended sediment ranges from 248 to 600 million tons per year, Meade, 1994; Martinelli et al., 1993; Filizola et al., 1999; Latrubesse et al., 2005). Other large tributaries such as the Negro, Tapajos, Xingu Rivers drain platforms or cratons in the savanna and rainforest and are characterized by low suspended sediment yields (ranging from 10 to 20 million tons per year, Filizola, 1999) compared to their enormous discharge rates and drainage area (Latrubesse et al., 2005). The scope of this study is the Amazon River in a basin-wide scale (bold-faced blue line in Figure 1); therefore in this study, spatial and temporal variations of surface sediment distributions based on the data supplied from different hydrometric stations over the entire mainstream of Amazon River are examined.

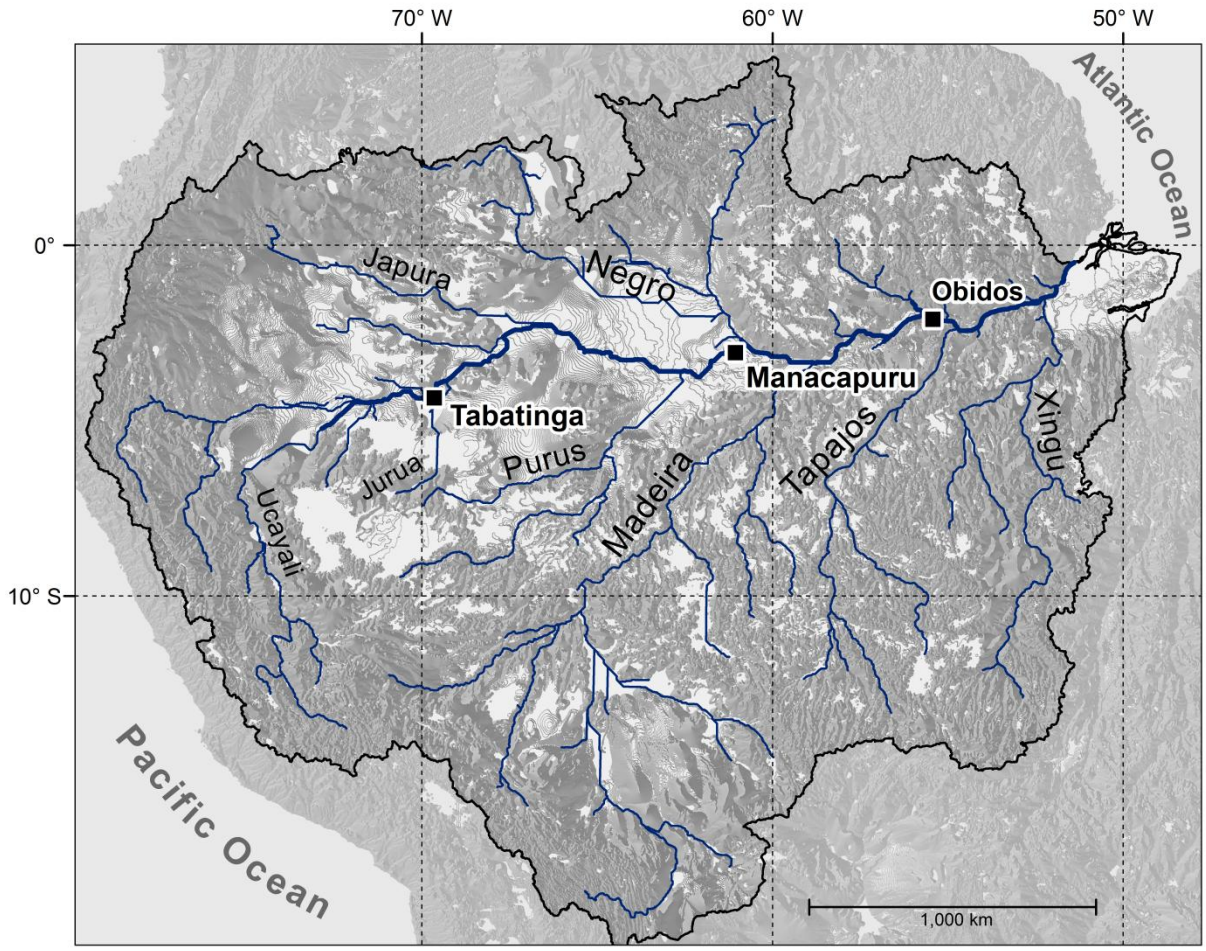

Figure 1. Map of the Amazon River and the major tributaries within the Amazon Basin (outlined). Amazon River (bold-faced line) marked by three gauging stations: Tabatinga; Manacapuru; and Obidos (halo-background) maintained by Brazilian Water Agency (ANA) are the research area of this study. Background aspect data was extracted from GTOPO30 Digital Elevation Model (DEM) developed by USGS EROS Data Center. Dashed-line grid (10° interval) represents each tile in MODIS Sinusoidal Tiling System. Two tiles are used in this study: 70-60°W, 0-10°S (h11v09) and 60-50°W, 0-10°S (h12v09).

Hydrometric stations

At present, the national hydrometric network is managed by the Brazilian Water Agency (ANA) and the database generated by the network is under the responsibility of the Brazilian National Electric Energy Agency (ANEEL). Hydrological data including water levels (cm), discharge rates (m^3/s), surface sediment concentrations (mg/l) and

Acoustic Doppler Current Profiler (ADCP) flow measurements for each station are organized and downloadable from the ORE-HYBAM website (http://www.ore-hybam.org/index.php). Daily water discharge rates (Q_d) measured at three different stations (i.e. Tabatinga, Manacapuru, Obidos) from 2000 to 2010 (available since 1972) were used in this study to define hydrological cycles around each station (Fig. 2, Table 1). These hydrological behaviors observed at different stations were analyzed to assess whether there is an effect of changes in water stage on sediment concentration rates and sensitivity of reflectance to remote sensing images (section 3.1.3). Significant yearly variations were not observed since the maximum different days of highs and lows between every year at each station were less than a month.

ORE-HYBAM has 38 network stations and performed 15 field campaigns to measure hydrological data since the 1990s. Among these, hydrological data from three stations, which are Tabatinga (4° 15' 0"S, 69° 55' 59"W), Manacapuru (3°19’37”S, 60°33’13”W) and Obidos (1°54’51”S 55°32’09”W), are used in this study. Since the focus of this study lies on the entire mainstream of Amazon River, three quite evenly distanced gauge stations[3] were selected in order to encompass the huge study area. In addition, selection of the three gauge stations was made in consideration of different characteristics of suspended sediment from different watersheds. As mentioned above, two largest contributing rivers in sediment transport in Amazon Basin are the Solimões River and the Madeira River (section 2.1.1). Hence, in order to compare the different

[3] Approximately, 1,000 km between Tabatinga and Manacapuru and 600 km between Manacapuru and Obidos.

properties of suspended sediment entering from different tributaries, Tabatinga and Manacapuru were selected to represent upstream of the Solimões River and downstream of Solimões River (before confluence with Negro River), respectively, while Obidos is assumed to capture the suspended sediment properties of Madeira River. Obidos has been considered as one of the most important gauge stations for suspended sediment in the Amazon Basin, as it is the first station after the confluence with Madeira River and the last gauge station along the Amazon River before its meeting with the Atlantic Ocean (Fig. 1). At Obidos, huge increases of water discharge and sediment concentration rates are observed compared to Manacapuru, because the two big tributaries enter into the mainstream of Amazon River: the Negro River; and the Madeira River[4] (Fig. 2).

[4] The Negro River, which is the largest black water in the world, contains low suspended sediments (Latrubesse et al., 2005), since it drains predominantly from tropical rainforest. In contrast, the Madeira River, draining directly the Bolivian Andes over a steep slope is a white river rich with suspended sediments. According to Filizola (1999), Madeira River is responsible for approximately the half of the total sediment discharge of Amazon River measured at Obidos (approximately 1200 million tons per year, estimated by Dunne et al., 1998), while it contributes 16 % of total water budget for Amazon River.

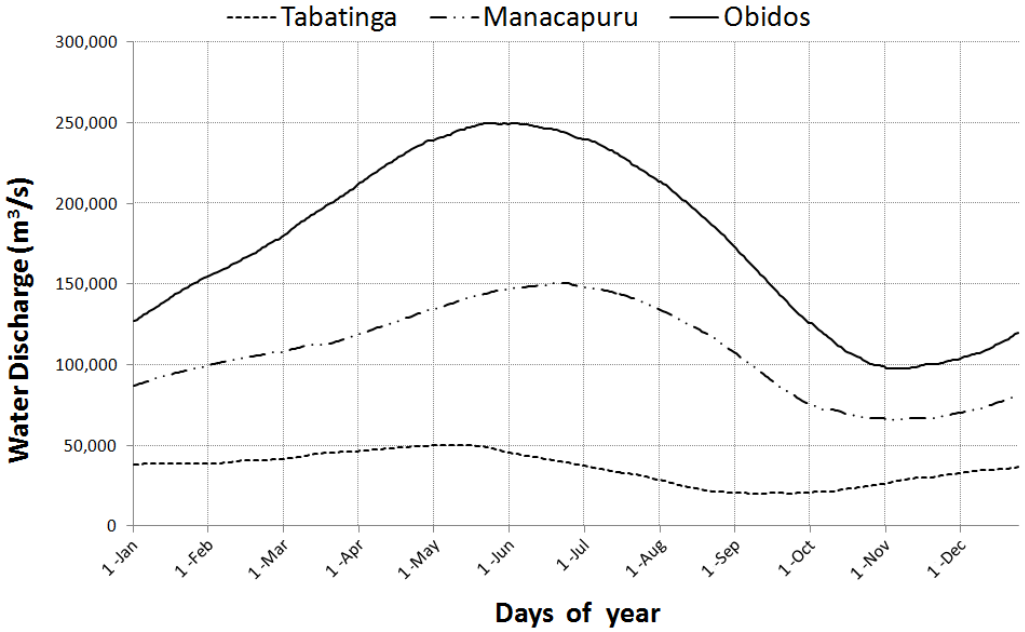

Figure 2. 11 years (2000 - 2010) average daily water discharge cycle for Tabatinga , Manacapuru and Obidos.

Station	Falling Period	Min	Rising Period	Max
Tabatinga	Jun - Sept	mid Sept	Oct - Apr	Mid May
Manacapuru	Jul - Nov	mid Nov	Dec - Jun	mid Jun
Obidos	Jun - Oct	early Nov	Nov - May	late May

Table 1. Summary of average hydrological cycles over 11 years at Tabatinga, Manacapuru and Obidos shown in Fig. 2.

2.2 DATA DESCRIPTION

MODIS Imagery

Various instruments have been implemented, such as Landsat, System for Earth Observation (SPOT), Sea-viewing Wide Field-of-view Sensor (SeaWiFS), Advanced Space borne Thermal Emission and Refection Radiometer (ASTER), and Moderate

Resolution Imaging Spectroradiometer (MODIS), for the estimation of sediments in rivers in different regions on Earth. This study implemented MODIS. MODIS, with a 2,330 km swath width, views the entire earth surface every one to two days providing the surface reflectance (REF) value for every corresponding ground measured surface sediment concentration (SSC) data that was gauged in an irregular time scale. Thirty-six bands from 0.4 to 14.4 µm with a narrow band width allow more precise measuring of surface reflectance rates than any other space imaging sensors.

A popular method relating the SSC rates in water surface and remote sensing uses the red portion of the visible spectrum, and was implemented in this study (Mertes et al., 1993). This is proven to be a reliable method because reflectance values recorded in remotely sensed imagery are often totally controlled by the scattering from suspended matters on the water surface when it is compared to pure water and phytoplankton absorption (Kirk, 1994; Mobley, 1994). Hence, the value recorded in satellite imagery and suspended matter on the water surface normally shows a robust linear relationship (Miller et al., 2004). There are four MODIS bands covering the spectral range between 0.6 to 0.7 µm: one medium-resolution (band 1); and three ocean bands (band 13, 14 and 27). Band 1 was exclusively used in this study to estimate surface sediments, because of its finest spatial resolution. Even though the ocean bands have higher sensitivity to detect subtle water properties, Band 1 is proven to provide sufficient sensitivity for surface water applications to detect changes in water-leaving radiances (Hu et al., 2004). Surface

reflectance (REF), highly sensitive to SSC rate, is recorded in a very precise manner with 16-bit quantization level scaling from -100 to 16000[5] in MODIS imagery.

Instantaneous Field Of View (IFOV) of 250 meters of MODIS is a moderate spatial resolution; however, it is considered to be suitable for this study because most of the reaches of Amazon River downstream of Tabatinga have widths greater than three kilometers, fitting more than 10 cells on average. The ratio of extent of a river to spatial resolution of a viewing remote sensor is defined as the scope by Schneider (2001), and normally a scope of 10 or greater is considered to be sufficient enough to retrieve valid information of the channel floodplain systems of large rivers (Mertes et al., 2007). Identical MODIS instruments are board two satellites: Terra (formerly EOS AM-1); and Aqua (formerly EOS PM-1). Both platforms are near-polar placed in circular sun-synchronous orbit but travel in opposite directions. The descending node Terra crosses the equator at approximately 10:30 AM in local solar time while the ascending node Aqua crosses the equator at approximately 1:30 PM in local solar time. Since the Amazon Basin is located around 2 - 3° S, both Terra and Aqua visit three gauging stations approximately between 10:30 AM to 1:30 PM when relatively high solar radiation is provided within a day. Therefore, it is possible to obtain two images during the daytime of the entire Amazon region every day.

However, due to frequent and heavy cloud cover in Amazon Basin, especially during the rainy season, 8-days composite MODIS products (i.e. MOD09Q1 (Terra)/MYD09Q1 (Aqua)), which consist of the highest quality pixels within successive

[5] Normally negative values are the fill values.

eight-days of daily surface reflectance products (i.e. MOD09GQ/MYD09GQ), were considered relevant to be associated with surface sediment in this study. These multi-day composite images are produced with the most cloud free pixels nearest to the pixels under the nadir out of all successive acquisition periods. The general characteristics (e.g. discharge, sediment concentration, and habitat characteristics) of many large rivers, which gradually change over time unless extreme natural hazards occur (Mertes et al., 2007) also supports the usability of MODIS 8-days composite surface reflectance product. In this sense, only a week of the possible maximum time lag between field sampling and satellite observation is assumed negligible. In addition, the 8-day composite product is relevant when retrieving the surface sediment concentration map over broad area (section 3.2) because normally it is difficult to acquire cloud free daily images along the Amazon River.

Two MODIS instruments mounted on Terra and Aqua started collecting earth surface data from early 2000 and the middle of 2002, respectively. In this study, both of MOD09Q1 and MYD09Q1 were utilized in order to procure as many samples as possible. The validations are as follows: MOD09Q1 and MYD09Q1 images could be considered as independent from each other. Although the two images' file names indicate the same date (raw HDF files are named after the 1st date of 8 successive dates), due to dynamically changing tropical climate, it is highly probable that two multi-day composite images' pixels for the same location were selected from different daily products (MOD/MYD09GQ). Even if the two images' pixels are selected from the same date, they are taken at different time (approximately 3 hours apart) within a day.

MODIS 8-day composite surface reflectance products cover the whole year. Hence, MODIS images were available for any date within a year regardless of the date of field sampling. Approximately four images were available every month for both MOD09Q1 and MYD09Q1 products. Thus, 1,980 images were downloaded for both scenes: h11v09 and h12v09 in MODIS Sinusoidal Tiling System (Fig. 1) from Land Processes Distributed Active Archive Center (LP DAAC, https://lpdaac.usgs.gov/) File Transfer Protocol (FTP) using Python[6]. For evaluation of pixels' quality, Quality Assurance (QA) information for MODIS land product (MOD/MYD09Q1 band 3) and solar zenith angle information from 500 meter spatial resolution 8-days composite MODIS product (MOD/MYD09A1 band 9) were separately secured. Both MOD/MYD09Q1 and MOD/MYD09A1 are level 3 (L3) products those are radiometrically and atmospherically corrected to yield surface reflectance and also precisely geo-located in a sinusoidal projection. After May 2008, all MODIS data became available in collection version 5 (V005), which yields the highest quality after comprehensive accuracy assessments and uses Hierarchical Data Format (HDF) keeping the data file size substantially smaller. MODIS products and their Science Data Sets (SDS) used in this study are summarized in Table 2.

[6] JPEG browse images were not checked in advance, since only a small portion of each scene (less than 100 pixels) was necessary around each station, which the quality is difficult to be assessed by visual inspection.

MODIS Products	MOD09Q1 MYD09Q1	MOD09A1 MYD09A1	MOD13Q1
Primary Uses	Land Cover, Vegetataion, Chlorophyll, Cloud Amount	Land Cover, Vegetation, Soil, Cloud	Vegetation, Water Property
Spatial Resolution	250 meter	500 meter	250 meter
Temporal Resolution	8-days Composite	8-days Composite	16-days Composite
Radiometric Resolution	16 bit (Fill = -1)	16 bit (0 - 180)	_
Total Number of Bands	3	13	12
Band Used	B1 (620-670 nm) B2 (841-876 nm) B3 (Quality Assurance)	B9 (Solar Zenith Angle)	B5 (841-876 nm)
Number of Images Used	1980 (together)	1980 (together)	264

Table 2. Summary of MODIS imagery used in this study.

Field measured surface sediment concentration data

The Environmental Research Observatory (ORE) - Geodynamical, hydrological and biogeochemical control of erosion/alteration and material transport in the Amazon basin (HYBAM) project was initiated by the French Ministry of Higher Education and Research and the Brazilian National Water Agency (ANA) in 2003 to provide the scientific community with the high quality data demanded to study and model the systems in the Amazon Basin. One of the research teams collaborating with ORE-HYBAM, the Laboratory of Mechanisms of Geology Transfer (LMTG) has been conducting researches in hydrological geodynamics in the Amazon basin since 1995 and collecting samples from 38 HYBAM network stations. Sediment concentration and water discharge data collected from the 15 field campaigns in the Amazon Basin needed for this

study were supplied from ORE-HYBAM web site (http://www.ore-hybam.org/index.php/eng/Data), which is freely available to public.

Surface sediment concentration sampling were taken in milligrams per liter (mg/L), approximately 2 to 4 times per month[7] at 12:00 PM from 2000 to 2010 from three sampling stations: Tabatinga (ORE-HYBAM station code 10100000); Manacapuru (14100000); and Obidos (17050001). Samplings of surface sediment were conducted by a local operator at approximately the middle of the river reach at a fixed point using a 500-milliliter bottle. Sampled bottles were sealed and sent to laboratories at the Brasilia University and the Amazonas State University for filtering. Laboratory filtrations were conducted using disposable sterilized filtration set with 0.45µm cellulose acetate membranes and dried to be weighed. For the detailed post-sampling protocol adopted by HYBAM, see GEMS/WATER (1994).

Field Data	Surface Sediment Concentration (mg/l)	Water Discharge (m^3/s)
Collecting Period	1995 - present	1972 - present
Temporal Resolution	Every 1st, 10th, 20th of month (at 12:00 PM)	Daily
Reponsible Agency	Environmental Research Observatory (ORE) - Geodynamical, hydrological and biogeochemical control of erosion/alteration and material transport in the Amazon basin (HYBAM)	Brazilian Water Agency (ANA), Brazilian National Electric Energy Agency (ANEEL)

Table 3. Summary of surface sediment concentration and water discharge data used in this study.

2.3 MODIS IMAGE PROCESSING

[7] Although slight irregularity in every 10 days of periodical gauging existed due to unavoidable cases, such as excessive flood or malfunction of gauging equipments. Complete section samplings were performed 2 to 4 times per year.

Figure 3 illustrates the framework of MODIS image processing to extract surface sediment concentration maps from 2000 to 2010. Three different kinds of MODIS products (MOD09Q1, MOD09A1, MOD13Q1) and five different types of bands were used to derive necessary information (Table 1). Prior to the image processing, only the MODIS 8-days composite images containing the date of field sampling of SSC data were stored separately to be used for calibration in this section (574, 621, 728 images respectively for Tabatinga, Manacapuru and Obidos). MODIS images that were not used for calibration with SSC data were also kept and have undergone the identical image processing process described in this section, since they should be used when generating maps of surface sediment concentration (section 3.2).

Since the red portion of visible electromagnetic spectrum is assumed to have a robust correlation with surface sediment concentration, MODIS's red band (MOD09Q1 band 1) was filtered using a water mask (MOD09Q1 band 2), quality assurance (MOD09Q1 band 3), and refined by solar zenith angle (MOD09A1 band 9) band. To generate surface sediment concentration maps (section 3.2), the Local Polynomial Interpolation (LPI) method was used to estimate the pixels still under the cloud cover after 8 days composition. These processes were implemented in ArcGIS 10 Model builder and iterated over the 11 years of the dataset (see appendix for model details).

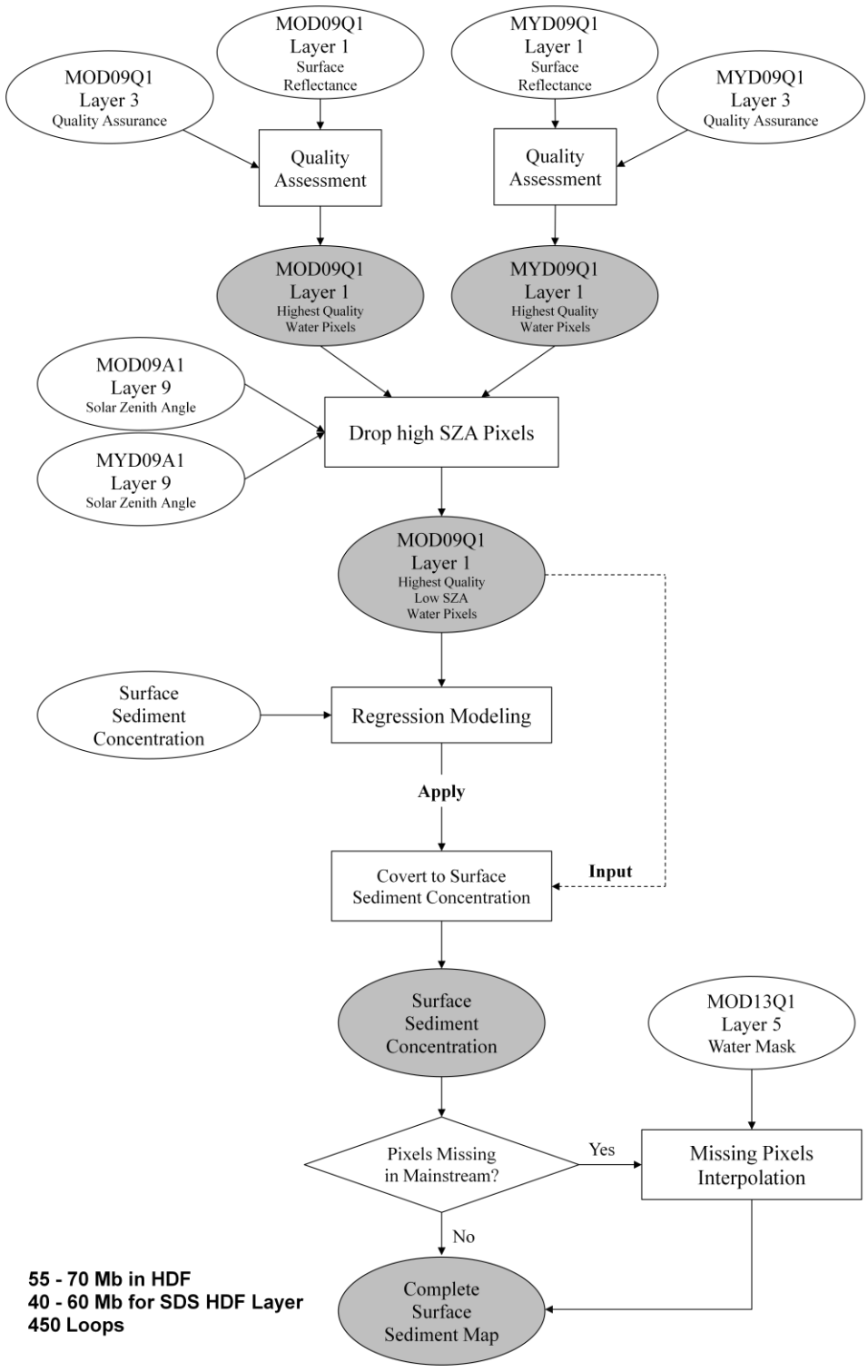

Figure 3. MODIS Image processing thread flow chart.

Image re-projection

Accurately determining specific pixels to be used in MODIS for calibration with field obtained data and projecting the river with the least distortion were essential parts of this study. For this reason, I changed the downloaded MODIS images to the sinusoidal projection based on World Geodetic System (WGS) 1984 by using the MODIS Re-projection Tool (MRT) available from LP DAAC website (https://lpdaac.usgs.gov/tools/modis_reprojection_tool). Sinusoidal Projection is a pseudo-cylindrical equal-area map projection where the vertical and horizontal scales are constant throughout the map and, hence, are used widely in the Amazon Basin with the WGS 1984 datum. To place the Amazon Basin at the center of the map, I changed the center of the projection's meridian to -60 degrees. MRT allows reading HDF formatted data files and specifies each science data sets (HDF layers).

Image pixel selection

Sites where field measurements were taken in the Amazon River were chosen in MODIS images around the sampled points. The sampling locations were geo-referenced from the documents "Descriptions of stations of sampling" for each station from the ORE-HYBAM website (http://www.ore-hybam.org/index.php/eng/choixstation/selbassin?list_sta=ref). Then, water outlines were manually sketched to cover the pixels around the center (sampled point) of the river. Homogeneous patterns of surface suspended sediment distributions were found after multi-directional visual inspections over MODIS and Landsat TM images for three regions during most of the time within year. However, to take into account the local and

momentary variations of surface sediment distribution which may be affected instantaneously by changes in tributary inputs from other basins and bank erosion rate, I maintained an extensive water mask[8]. An expansion of few pixels from the sampling point is not considered to cause a significant loss of information, because pixels in the extracted water mask exhibit strong spatial autocorrelations with their adjacent pixels across the river surface. Also, in such a large river like the Amazon River mainstream, even with highly accurate Global Positioning System (GPS) units, spatial variability in the sampling points might exist, especially during the rainy season when the river becomes more dynamic.

Different numbers of pixels (40~70) were used depending on the local geologic-geomorphologic features around the river where samples were taken. When sketching the outlines of river masks, Landsat 5 Thematic Mapper (TM) images of similar dates were used to supplement moderate spatial resolution of MODIS images. Selected pixels are considered to represent the continuous and slowly changing surface sediment distribution over the river surface.

Spectral mixture analysis

At the Manacapuru and Obidos gauge stations, widths passing through the sampling points are approximately four km and three km respectively, which are wide enough to have appropriate scopes even by a moderate resolution remote sensor. Therefore, sufficient numbers of pixels exist to cover the sampling points and

[8] Too small number of pixels could be susceptible to small spatial and temporal variations and prone to lose significant amount of pixels after masking out disqualified pixels.

surroundings despite high spatial variations of surface sediment distributions (Filizola et al., 2009). However, the width of the river at Tabatinga gauge station is around 1 km, which is relatively narrow, laterally fitting five complete pixels at maximum (not partially overlaid). Therefore, I decided to perform spectral mixture analysis for the pixels partially overlaying on land to extract the pure spectral characteristics of the water in order to secure the maximum number of pixels possible around the sampling point at Tabatinga station (Fig. 4). Although mixed pixels at the boundary of the water mask is several hundred meters away from the SSC sampled point, they are still considered to represent conditions of surface sediment of the sampled point because surface sediments are detected to be substantially homogeneously distributed across the river. A homogeneous distribution of SSC is proven by both ways: examining ranges of standard deviations of all pre-unmixed water masks (0.002 – 0.025 (reflectance)) and visual inspections on several MODIS and Landsat 5 TM images.

Novel linear unmixing of pixels to retrieve pure water characteristics was performed for these boundary pixels. True color Landsat 5 TM images on a close date were used to determine end-members. End-members were estimated by careful observation of the scenes since defining representative physical component on land those have a representative spectral characteristics is a key for linear spectral mixture analysis. Vegetation is dominant on both sides of the river; and quite intense urban developments were scattered in a small municipality of Tabatinga on the left bank. In addition, sand features were obviously detected along the edge of the river. End-member characteristics were derived from homogeneous and large featured areas for each class near Tabatinga

region. Then, TM images were classified using a supervised classification method based on spectral characteristics of these four end-members. Then, I used the TM-derived classified map to determine location and calculate area of each class. Pure water characteristics were retrieved using the formula below (eq. 1).

$$REF_{(x,y)} = \left(\frac{1}{250}\right)^2 \cdot \sum (REF_i \cdot A_i)$$

Equation 1. Spectral mixture analysis model implemented in Tabatinga.

$REF_{(x, y)}$ denotes the pixel reflectance value to be unmixed in MODIS image at an x, y coordinate while REF_i, A_i refers to the reflectance characteristics and area of each class respectively. Subscript i refers to four defined classes, which are water, vegetation, soil and urban features. This method of spectral mixture analysis does not require additional bands unlike typical spectral mixture analysis methods, even if there are more than four classes.

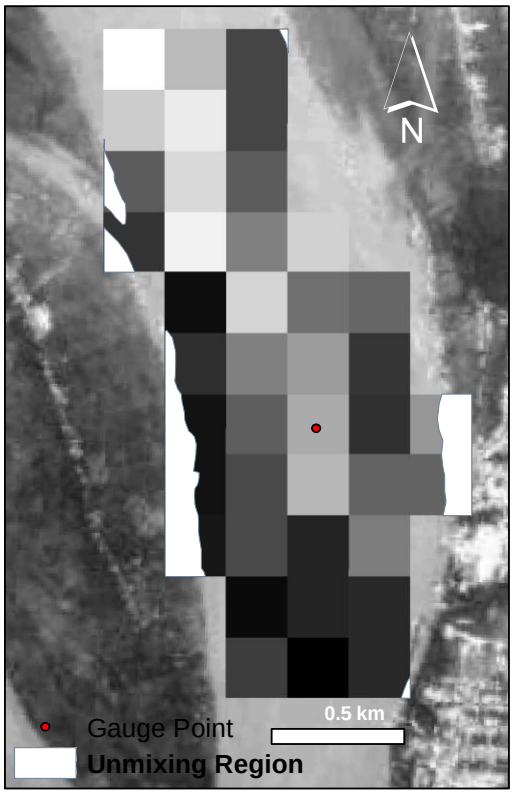

Figure 4. Graphical overview of the regions where spectral mixture analysis was applied in Tabatinga gauging site superimposed on higher spatial resolution Landsat 5 TM imagery.

Quality assessment

Along with surface reflectance bands, the MODIS Quality Assurance (QA) information band from MOD/MYD09Q1 was used to assess the per-pixel quality for every layer. Quality Assurance information is an essential part of the MODIS Surface Reflectance products, and it is normally stored as metadata to document the scientific quality of each pixel. The QA layer was decoded by using particularly the unpack_sds_bits utility available from https://lpdaac.usgs.gov/tools/ldope_tools. Decoded layers composed of integer numbers were loaded into the software ERDAS Imagine 2010

and interpreted in conjunction with the MODIS surface reflectance band quality description (Vermote et al., 2011). Only the pixels in the Band 1 with the highest quality (where bit number 4 to 7 is '0000') were masked out to be correlated with the field measured sediment data.

Water masks were discarded for the remaining pixels after the masking out process were less than half of the original masks. Band 1 was then multiplied by its scale factor (0.0001) to retrieve surface reflectance values and archived in Tagged Image File (.tif) format. A total of 287, 241, and 324 images were available respectively from Tabatinga, Manacapuru, and Obidos stations after filtration was performed based on QA information. Total possible QA bit numbers information and their acceptance are summarized in Table 4.

After the filtering of high quality pixels through MODIS QA band, the relative location of the sun at the time each pixel value was obtained must be considered since each pixel has a relatively different Solar Zenith Angle (SZA) depending on the time of day and season within the year when surface reflectance was recorded. Solar Zenith Angle may have a significant effect on pixel value because the surface data collected with a large SZA would be more affected by Rayleigh scattering effects, since the light waves reflected from the sun would have to pass through a larger volume of atmosphere (Vermote et al., 1999). Therefore, it is reasonable to compare images taken on the same date and drop images acquired at substantially high SZA. SZA information was extracted from the MODIS 500 meter 8-days composite product (MOD/MYD09A1) and resampled to 250 meter spatial resolution using the nearest neighbor interpolation technique to be

comparable with 250 meter 8-days composite product (MOD/MYD09Q1). ArcGIS 10 Spatial Analyst Raster Calculator was implemented to drop pixels with substantially high SZA from MOD/MYD09Q1 and created new combined images with only pixels that had a relatively low SZA. For some locations where only one of the two pixels (MOD/MYD09Q1) was remaining even before examining SZA, an existing value was kept because the SZA for both Terra and Aqua are both not significantly high in any cases (< 38 degrees). In addition, the red band has relatively low variability depending on SZA (Galvao et al., 2011). After dropping images with high SZA, 267, 232, and 318 images remained for each gauging station to be correlated with surface sediment concentration data.

Singed Integer	Bit string (Binary)	Accepted
3811	0000 1110 1110 0011	X
4096	0001 0000 0000 0000	O
4305	0001 0000 1101 0001	X
4323	0001 0000 1110 0011	X
7425	0001 1101 0000 0001	O
7633	0001 1101 1101 0001	X
7683	0001 1110 0000 0011	O
7891	0001 1110 1101 0011	X
20480	0101 0000 0000 0000	O
24067	0101 1110 0000 0011	O

Table 4. Summary of possible QA bit numbers for MODIS imagery used in this study. Refer to Vermote et al., (2011) table 13.

2.4 DATA AVAILABILITY

After MODIS image processing, a substantial amount of remotely sensed images still have to be obtained to be regressed with SSC (267, 232, 318 images for each of three regions). However, temporal variations of remotely sensed data availability exist in each region (Fig. 5) and their availability patterns influence the selection of datasets to be used in regression modeling.[9] Therefore, it should be observed that using whole selected samples might lead to a potential bias in the model because the selection process (i.e. availability of data more pronounced during particular season) is correlated with the response variable REF.

Although the total number of images available for each station is different, interesting patterns were observed. Tabatinga showed an obvious pattern in that most of the available images fell into rising stage of discharge and dramatically decrease from the discharge peak and, eventually ,a few images are available in the dry season (June - September) (Fig. 5). This suggests that, despite the onset of the dry season, atmospheric conditions still interrupt the remote sensor to properly capture the surface reflectance. According to the Figure 4 in Kilham et al. 2011 (see Appendix), the image availability is lowest from late March to June, when there is the greatest local rainfall in this part of the basin, and the number of available images was relatively evenly distributed among other months. Among my three study regions, Tabatinga and Mancapuru showed similar image available pattern with Kilham et al's. In fact, I examined image availability for each three separate regions (Fig. 5) while Kilham et al's analysis was based on entire Amazon.

[9] Reflectance value derived from remote sensing imagery is set as dependent variable in regression model (section 3.1).

Considering Amazon's enormous spatial scale, different regions could have season-dependent specific atmospheric conditions, which affect the availability of remote sensing images. At the downstream Obidos, nearly twice the total number of images were available compared to Tabatinga, which is the most upstream region. This difference is mainly caused by their different river width that, wide reach at Amazon River's downstream reduced the risk of cloud disturbance seen at Tabatinga or Manacapuru.

Sampled roughly on 1st, 10th and 20th of every month from 2000 to 2010, unlike the MODIS imagery, SSC data does not show explicit patterns of availability suggesting that data availability of SSC do not have a significant influence on the selection of total available data[10]. However, there are a few years containing certain periods (over 6 months) when operators failed to sample data due to various reasons, such as local weather condition or malfunction of machinery. In order to minimize the bias in regression models taking into consideration of irregular availability of SSC samples, I discarded entire SSC samples from those years when unsampled periods exceeded 6sixmonths within a year. Table 5 (a) summarized total available datasets per month after discarding data in biased years for 11 years from 2000 to 2010.

[10] Surface sediment concentration value sampled from field is set as independent variable in regression model (section 3.1).

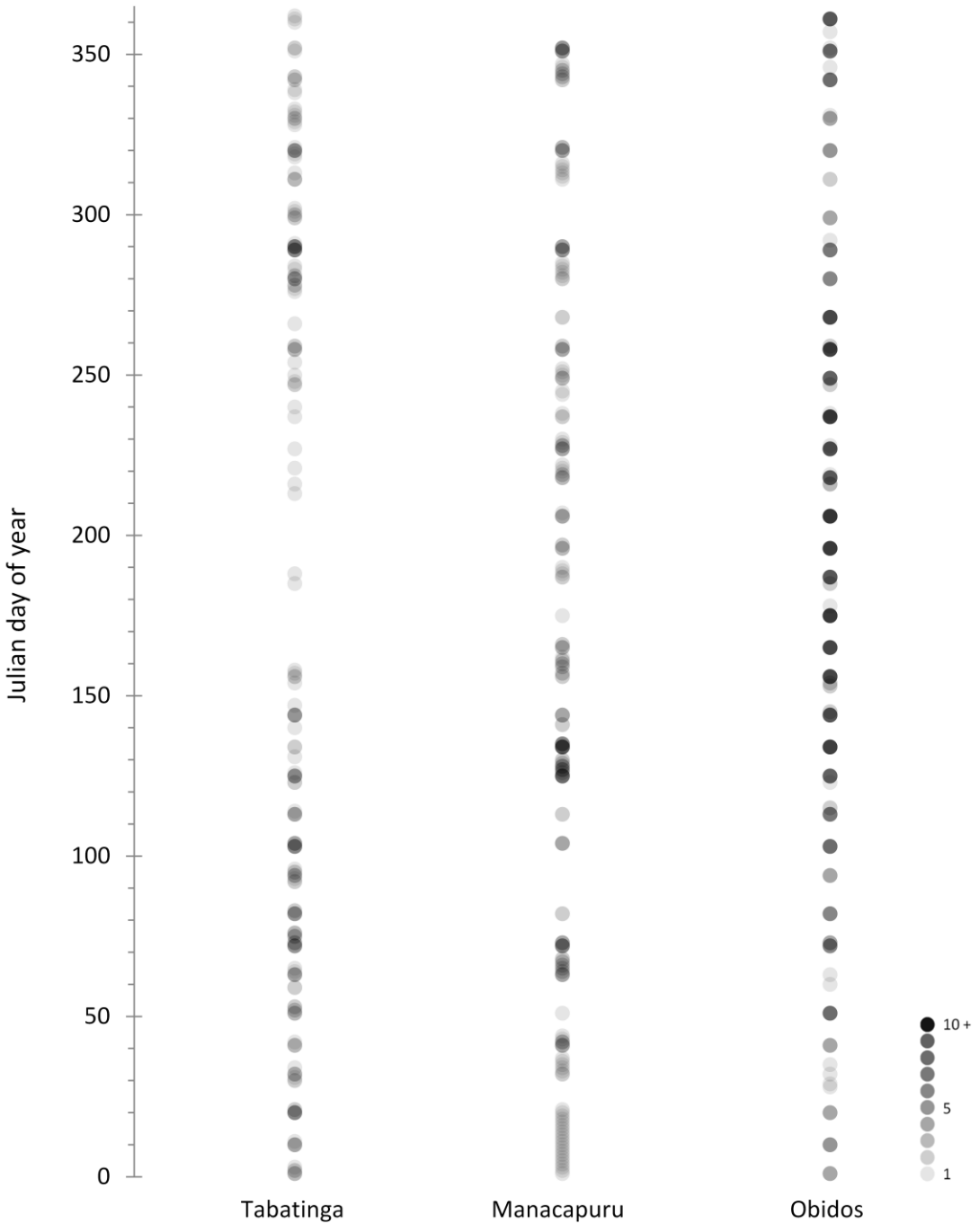

Figure 5. Dispersion plot showing data availability of number of total MOD09Q1 dataset over 11 years (2000-2010) from three regions.

Month	Tabatinga	Manacapuru	Obidos
January	21	21	15
February	20	17	13
March	26	26	15
April	27	24	21
May	19	24	38
June	3	20	41
July	6	12	42
August	6	21	33
September	10	16	36
October	30	18	18
November	21	13	12
December	18	20	29
Sum	207	232	313
Mean	17.25	19.33	26.08
Std.dev	8.96	4.33	11.6

Table 5(a). Summary of total available datasets per month for each station after quality testing for 11 years from 2000 to 2010.

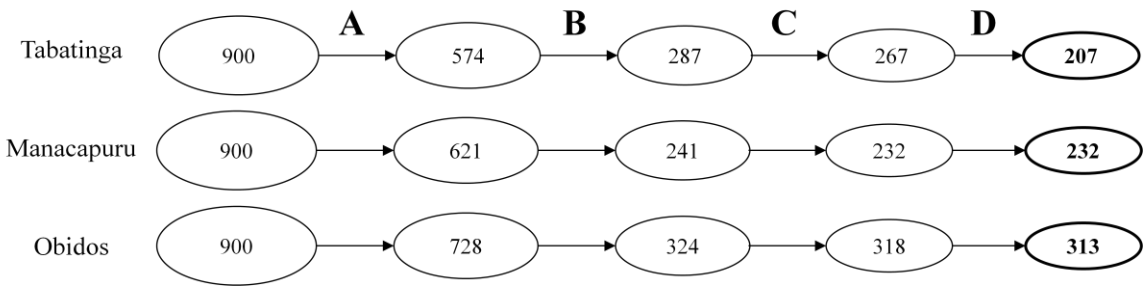

Table 5(b). Summary of filtration processes and number of datasets after each step. **A**: Initial filtering of remote sensing images acquired at the same date with field sediment sampling; **B**: Quality Assessment; **C**: Solar Zenith Angle; **D**: SSC dataset available over 6 months of every year.

Chapter 3: Results

3.1 PROCESSED DATA ANALYSIS

Since samples used in this study were measured from three gauging sites, it is necessary to validate the comparability of three groups of samples. If samples are proven to behave distinctly from each other, it is also necessary to investigate how the datasets should be temporally segmented within each site. In order to prove the compatibility of data from three sampled sites, I carried out statistical analyses using the R statistical package (http://www.r-project.org/).

Linear models from different sampling regions

In this part, one of the specific goals towards the ultimate objectives (analysis of mega-pattern sediment distribution) is summarized, which tries to build a linear model showing the relationship between surface sediment concentration and reflectance. As described above, this part aims to make an accurate linear model between SSC and REF that will eventually allow the prediction of SSC quantity as long as the REF value is available. Since sediment from a basin is expected to have similar mineralogical properties (Mertes et al., 1993; Martinez et al., 2009), I plotted two quantitative variables for three sampled locations by setting REF as a responsive variable and SSC as an explanatory variable as the first step for getting an insight into the relationship between SSC and REF (Fig. 6). The reason that I set REF as a dependent variable is because the reflectance value recorded at each pixel in MODIS image is determined by the quantity of SSC at particular location. Since this part aims to calibrate model of REF and SSC, it

is relevant to set REF as the dependent variable in order to see how REF varies as a function of field measured SSC values. However, the models generated in this section are inverted to predict SSC based on REF when generating SSC maps (section 3.2). The regression equation was determined to be y = 0.00111x + 0.0364 with 0.911 for the coefficient of determination (R^2).

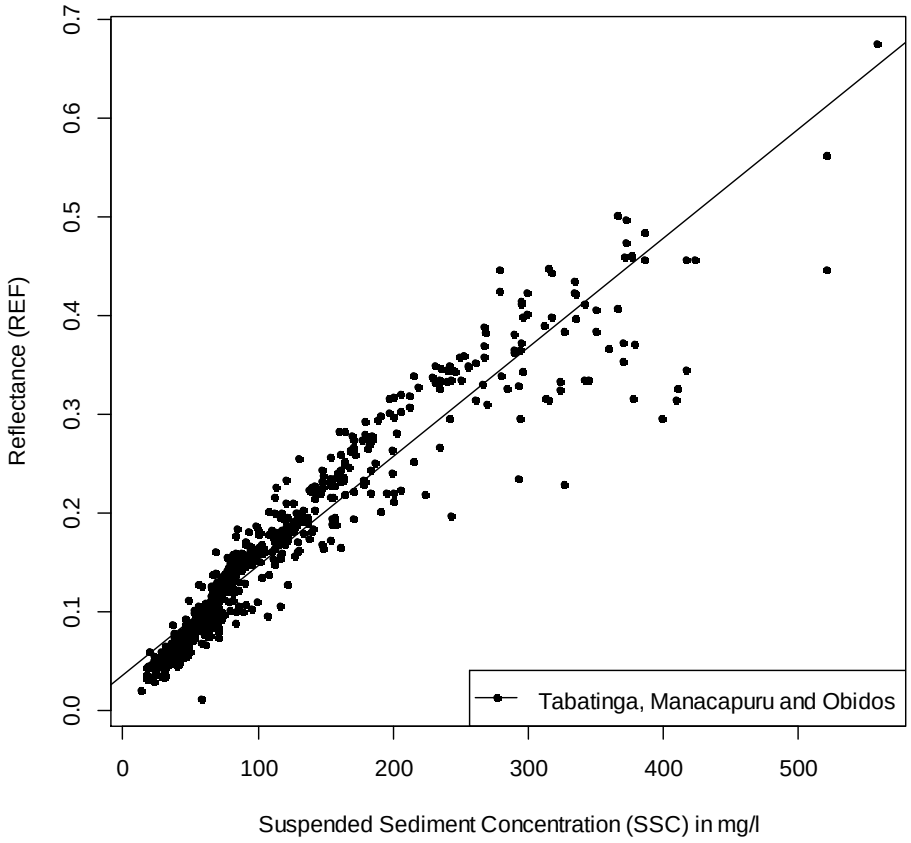

Figure 6. The regression between SSC and REF for combined data from sampled station: Tabatinga, Manacapuru, and Obidos.

The next step was to examine regressions individually between SSC and REF for Tabatinga, Manacapuru and Obidos to see if three regressions show different relationships between SSC and REF. This is necessary because it may not be ideal for generating a single linear model by combining three data sets from heterogeneous regions assuming that REF's behavioral pattern in response to the SSC value is distinct depending on regions. Figures 7(a), 7(b) and 7(c) show the regression between SSC and REF for Tabatinga, Manacapuru and Obidos, and the equations are $y = 0.001x + 0.057$ ($R^2 = 0.881$), $y = 0.00153x + 0.0118$ ($R^2 = 0.864$) and $y = 0.00135x + 0.0112$ ($R^2 = 0.904$) respectively. Substantially high coefficient of determinants were observed from all three regressions suggesting that REF is likely to be well-predicted by the SSC value by utilizing linear regression models. The same x-axis and y-axis scale was used to plot three different data sets in order to show individuals' data distribution under each other's relations.

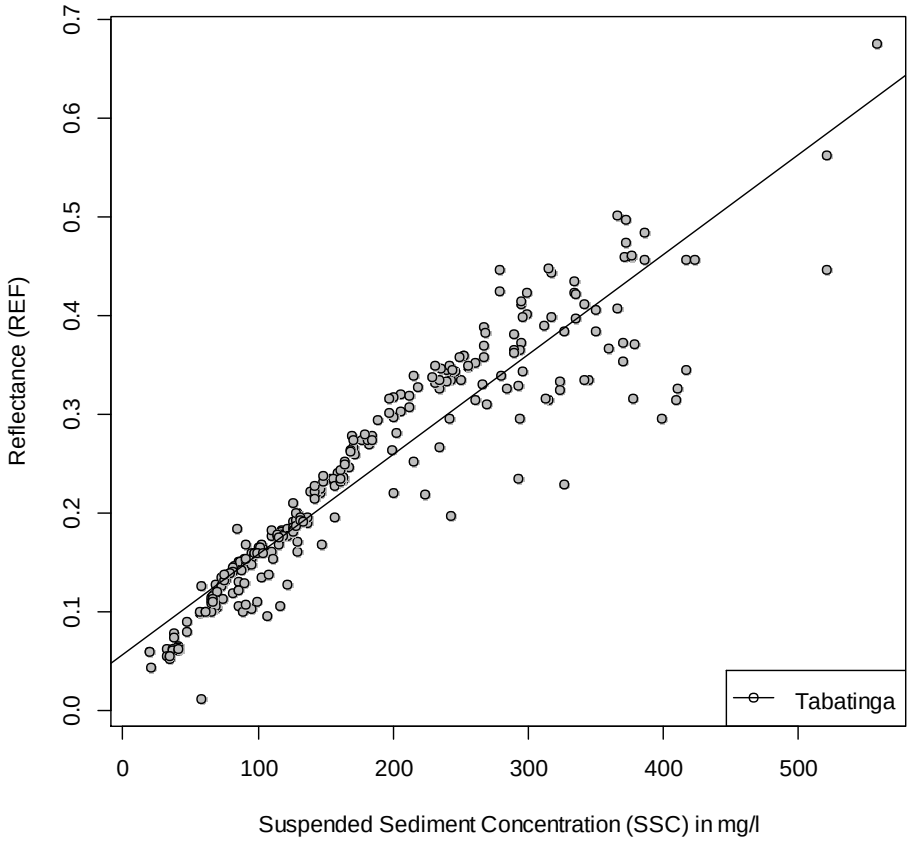

Figure 7(a). The regression between SSC and REF for Tabatinga.

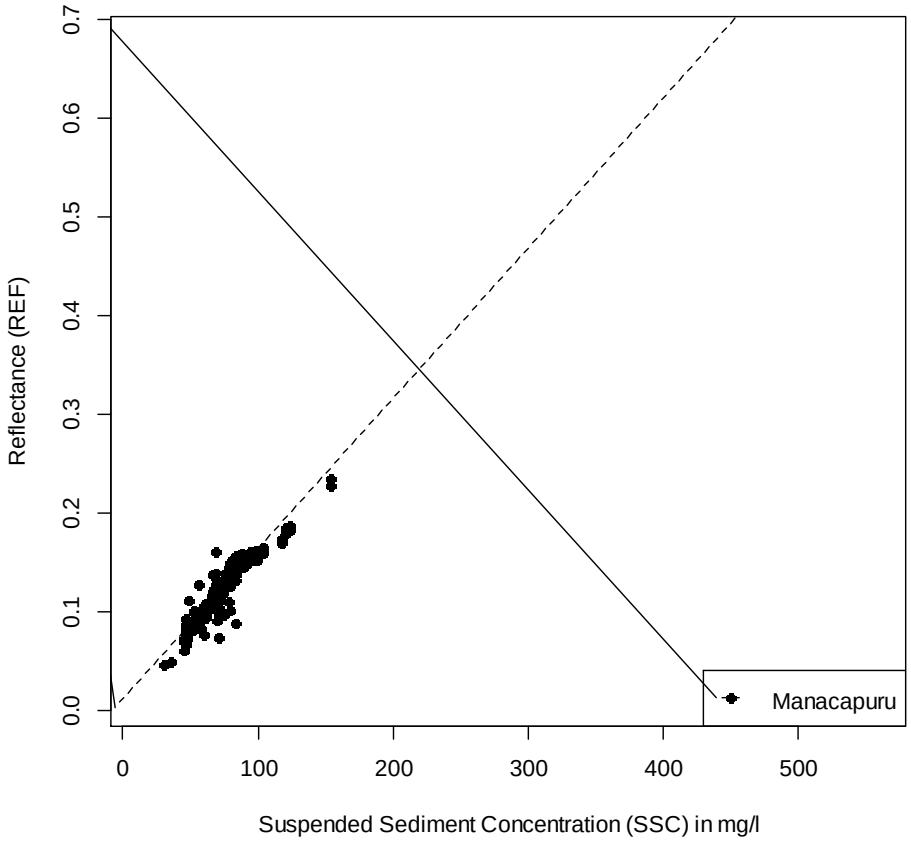

Figure 7(b). The regression between SSC and REF for Manacapuru.

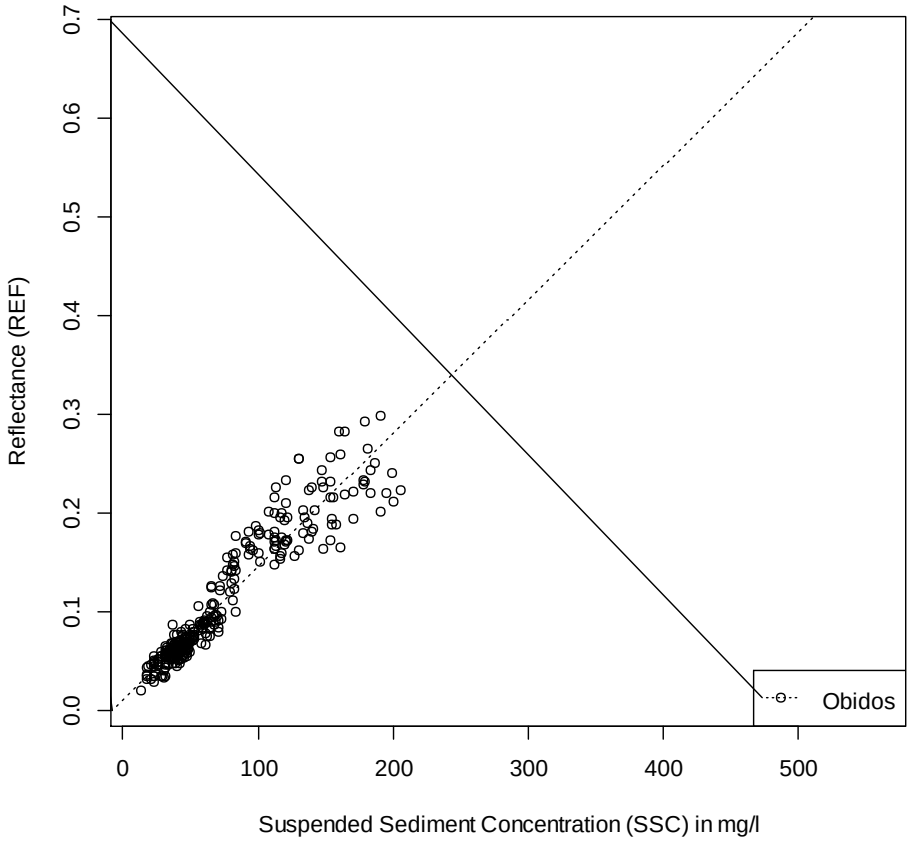

Figure 7(c). The regression between SSC and REF for Obidos.

Although similar characteristics of sediment are expected from the same basin, due to the extensiveness of Amazon Basin and impacts from tributaries, three regression models (in Fig. 7) were compared using the Analysis of Covariance (ANCOVA) at 0.05 α-level. The ANCOVA is a widely used method for testing differences in slopes and intercepts among regression models by testing the effect of a categorical variable on a response variable while controlling for the effect of a covariable. In this study, direct

correlation between the reflectance value recorded in satellite imagery and the surface sediment concentration rate in particular day is validated. Hence, region, which here, consists of three levels- Tabatinga, Manacapuru and Obidos- is defined as categorical variable, reflectance is defined as response variable and surface sediment concentration defined as covariable to be used in ANCOVA.

Table 6 shows the result of the ANCOVA tested for three different regressions shown in Figure 8. The ANCOVA result shows high significant effects of SSC and REGION on REF ($p < 2e - 16$, $p = 2.68E - 11$ respectively). However, the result also shows the significance of the interaction between SSC and REGION on REF ($p < 2e - 16$), which indicates that the slopes of the regressions between SSC and REF are not similar for Tabatinga, Manacapuru and Obidos. Clear existence of an interaction term between SSC and REGION failed testing the main effect of SSC on REF. To verify their interactions, the relationship between SSC and REGION should be investigated by individual examinations of three models from different gauging stations.

	Df	Sum Sq	Mean Sq	F value	Pr(>F)
SSC	1	7.553	7.553	10292.75	< 2e-16
REGION	2	0.037	0.018	25.06	2.68E-11
SSC:REGION	2	0.079	0.04	53.91	< 2e-16

Table 6. The ANCOVA result.

Testing models in common SSC range

I reasoned that the observed differences might be attributed to the huge discrepancies in properties of samples obtained from heterogeneous regions. For example, the number of samples available for this study is different from regions: 207 for Tabatinga, 232 for Manacapuru and 313 for Obidos, which might lead to biased results. Also, Manacapuru and Obidos show a quite narrower range of SSC and REF than Tabatinga, and even Manacapuru's Inter-quartile range (IQR) does not show any overlap with IQR of Tabatinga (Fig. 8(a), 8(b)). This phenomenon is more prominent in terms of SSC values, which perhaps manifest in the different nature of three gauging stations.

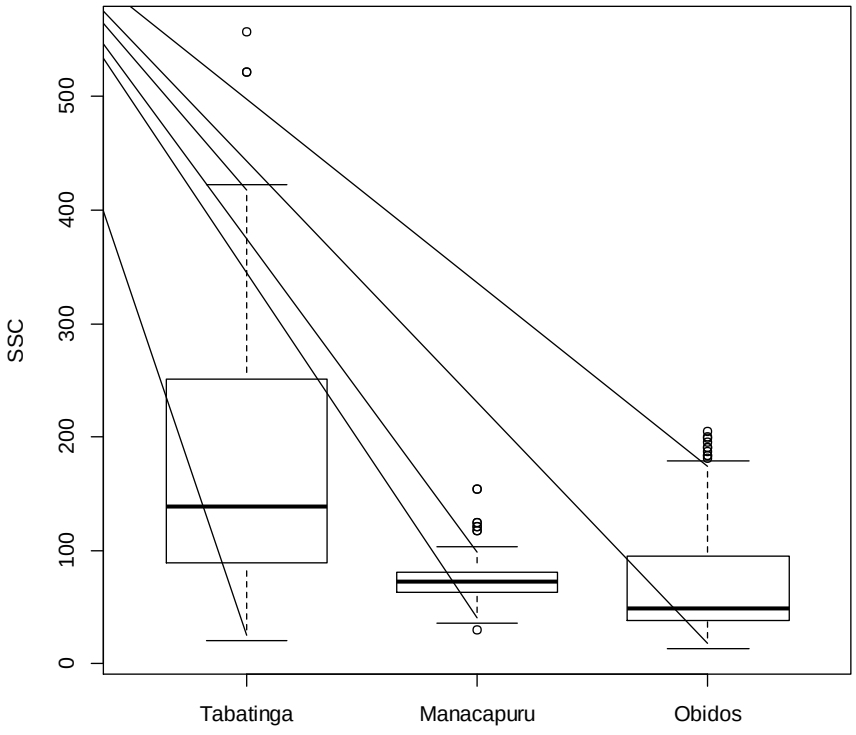

Figure 8(a). The range of SSC for Tabatinga, Manacapuru and Obidos. The first quartile (Q1), the second quartile (median) and the third quartile (Q3) of the SSC range for Tabatinga is 88.5, 138.8, 251.2

respectively and 63, 72, 81 respectively for Manacapuru. Also, the Q1, median, Q3 of the SSC range for Obidos is 38.5, 49.3, 94.9 respectively.

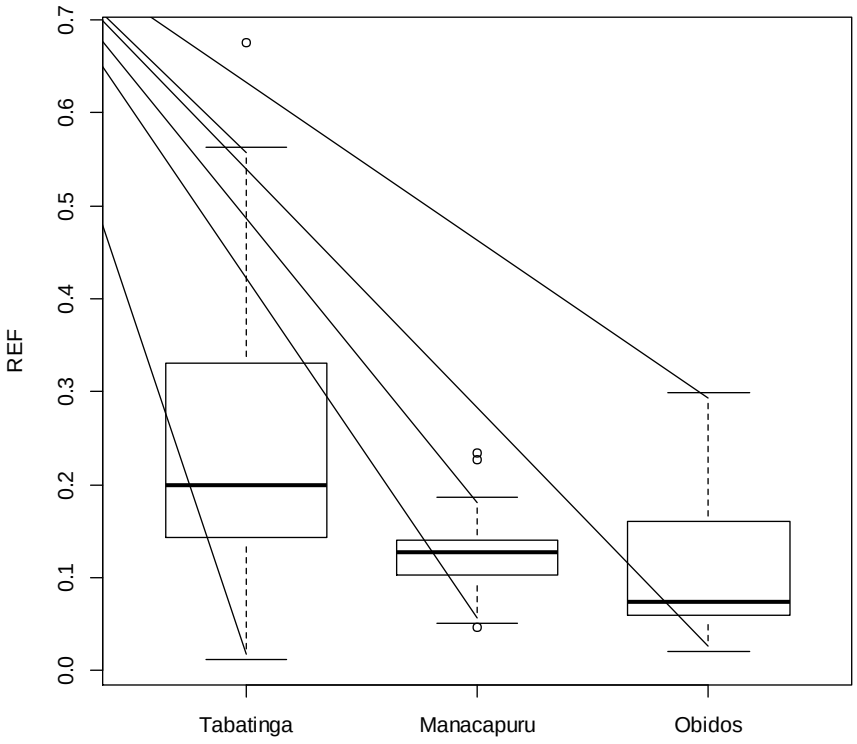

Figure 8(b). The range of REF for Tabatinga, Manacapuru and Obidos. The Q1, median Q3 of the REF range for Tabatinga is 0.144, 0.2, 0.331 respectively and 0.103, 0.127, 0.14 respectively for Manacapuru. Also, the Q1, median, Q3 of the SSC range for Obidos is 0.059, 0.075, 0.16 respectively.

These inconsistent characteristics of samples between Tabatinga, Manacapuru and Obidos are likely to prevent a fair comparison between regressions. Hence, to control these impedient factors, I investigated the regressions by considering the subsets of sampled data whose SSC range is common for all three regions. This step is necessary

since the range of measured SSCs for each station show quite different characteristics (Fig. 8(a)). Manacapuru, especially, shows only a limited range which completely overlays the SSC ranges of Tabatinga and Obidos (Fig. 8(a) center box plot). For this analysis, I clipped out the subsets of Tabatinga and Obidos data sets whose SSC range is between 30 mg/l (minimum SSC rate for Manacapuru) and 154 mg/l (maximum SSC rate for Manacapuru). Then, regression equations between SSC and REF of a common range were derived for Tabatinga and Obidos: $y = 0.00135 + 0.0186$ ($R^2 = 0.847$) and $y = 0.00154x + 0.00079$ ($R^2 = 0.907$) respectively. Two regression models together with the original regression model from Manacapuru (regression model for Manacapuru did not change because the SSC range remained unchanged) seem more similar compared to what was observed in Figure 9 (Fig. 7). Finally, three regression models were compared using ANCOVA (Table 7). The ANCOVA result shows significant effects of SSC and REGION on REF, as well as significant interactions between the REGION and SSC on REF (($p < 2E - 16$, $p = 6.17E - 15$, $p = 0.000325$ respectively) which suggest that the regression models from Tabatinga, Manacapuru and Obidos are not comparable. Although the interaction term between REGION and SSC affecting REF is less significant in the common SSC range (Table 7) than in the entire SSC range (Table 6), the observed dissimilarities in the relationship between SSC and REF restricts the utilization of coupling linear models from different regions.

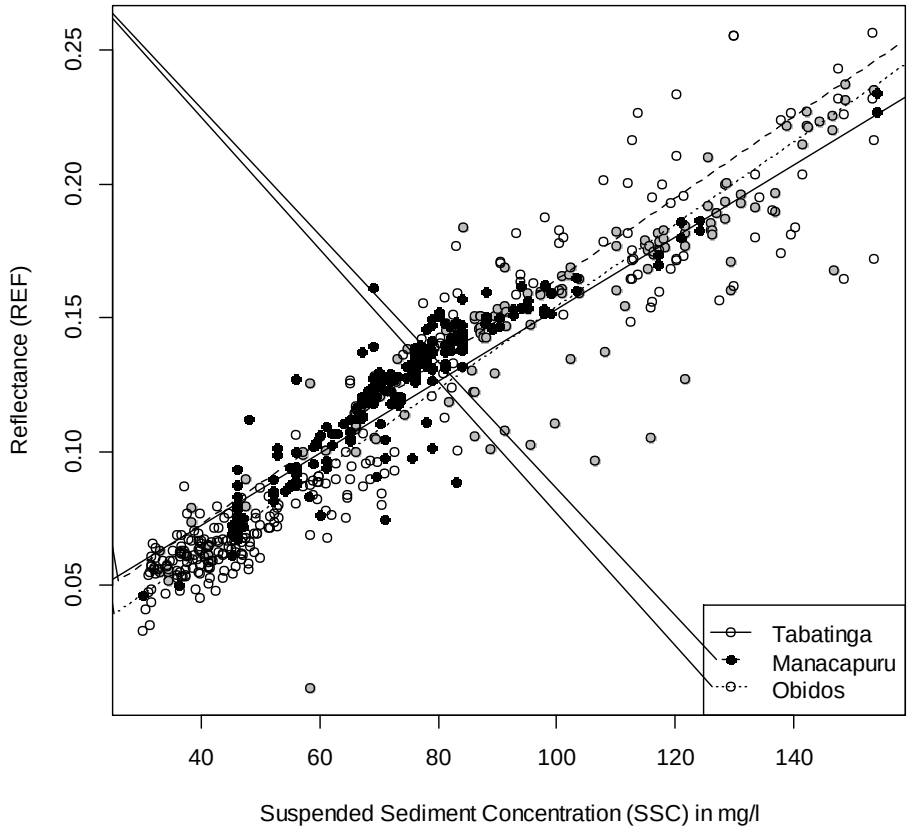

Figure 9. The regression between SSC and REF for Tabatinga, Manacapuru and Obidos.

	Df	Sum Sq	Mean Sq	F value	Pr(>F)
SSC	1	1.3268	1.3268	5858.69	< 2e-16
REGION	2	0.0156	0.0078	34.401	6.17E-15
SSC:REGION	2	0.0037	0.0018	8.129	0.000325

Table 7. The ANCOVA result for shared SSC range.

Testing effects of hydrological cycle

Given the observation that REF values respond in distinct manners for similar SSC values depending on regions, the next step was to investigate which factors are affecting the relationship between SSC and REF. The previous research conducted at Madeira River (Villar et al., 2012) provided me with one clue that the temporal variations (i.e. based on hydrological cycle) of spectral response from SSC might exist also in Amazon River, since light absorption and scattering is a function of particle concentration, size distribution and refractivity (Forget et al., 1999), which vary seasonally in the Amazon River.

As an extension from this reasoning, I plotted water discharge (Q) and SSC that were measured at a regular time scale from January 2000 to December 2010 for Tabatinga (Fig. 10(a)), Manacapuru (Fig. 10(b)) and Obidos (Fig. 10(c)). Obidos shows a clear pattern that SSC similarly fluctuates to the hydrological cycle (Fig. 10(a)). Also, similar patterns are shown in Tabatinga and Manacapuru (Fig. 10(b) and 10(c), respectively). In summary, SSC level is affected by the hydrological cycle, and their temporal variation patterns across the whole Amazon River tend to be similar. Hence, it becomes necessary to examine the association of REF and SSC based on this pattern.

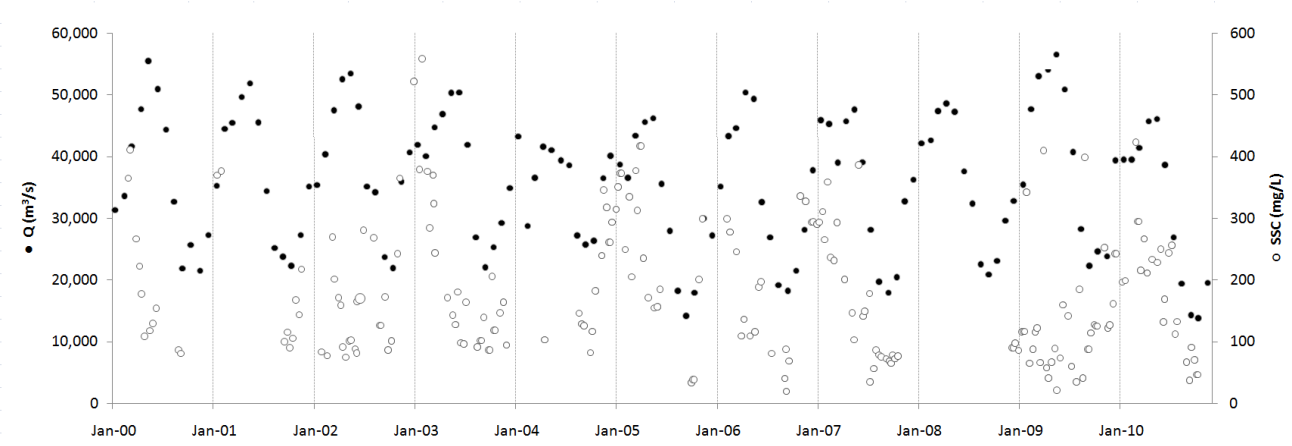
60,000
50,000
40,000
30,000
20,000
10,000
0
Q (m³/s)
600
500
400
300
200
100
0
SSC (mg/L)
Jan-00
Jan-01
Jan-02
Jan-03
Jan-04
Jan-05
Jan-06
Jan-07
Jan-08
Jan-09
Jan-10

(a)

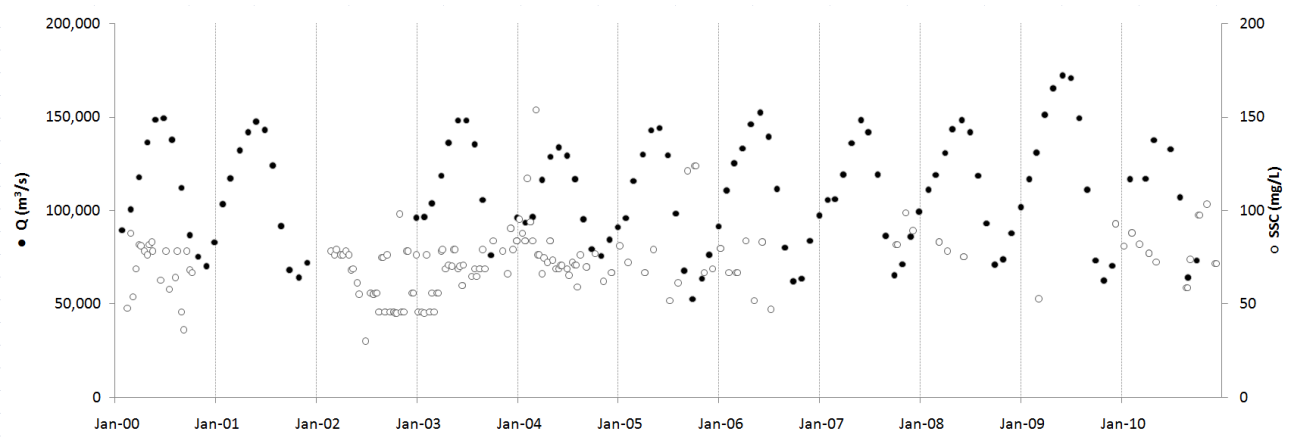
200,000
150,000
100,000
50,000
0
Q (m³/s)
200
150
100
50
0
SSC (mg/L)
Jan-00
Jan-01
Jan-02
Jan-03
Jan-04
Jan-05
Jan-06
Jan-07
Jan-08
Jan-09
Jan-10

(b)

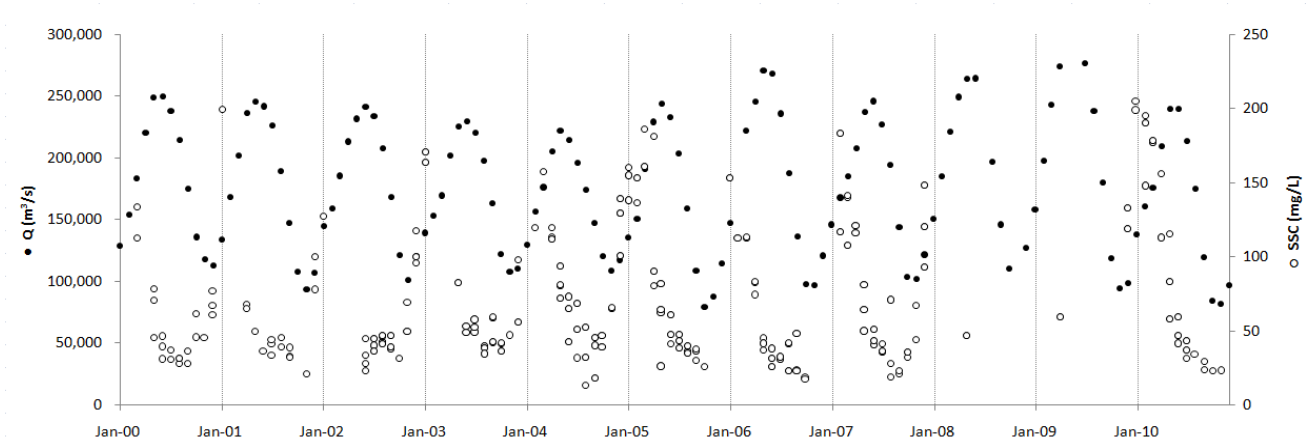

(c)

Figure 10. The hydrological cycle and SSC for three regions: Tabatinga (a), Manacapuru (b) and Obidos (c). Note the different scales in y-axis between regions.

To test the effect of the hydrological cycle on SSC, I split each dataset into two subsets based on the hydrological cycle (Table 2). Then, box plots were generated to see how different the distributions of SSCs are from rising stage to falling stage (Fig. 11(a), (b) and (c)). The difference in SSC depending on the hydrological cycle appeared to be highly significant for Obidos ($p < 2.2e - 16$) (Fig. 11(c)), Manacapuru ($p = 5.991e - 05$) (Fig. 11(b)) and Tabatinga ($p = 2.04e - 05$) (Fig. 11(a)), which confirms that the SSC levels are highly susceptible to changes in the hydrological cycle at all three stations.

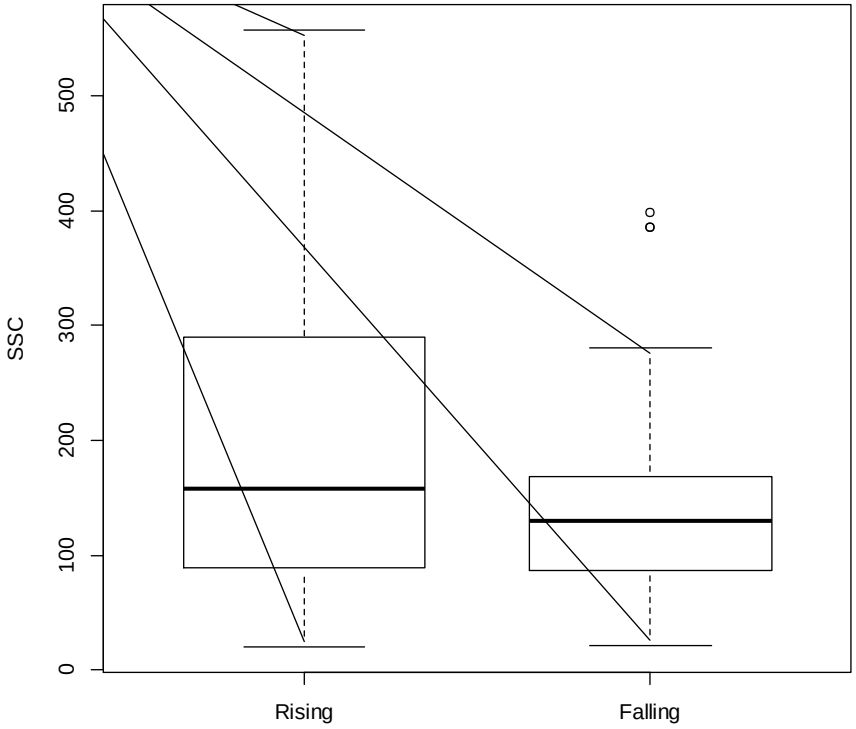

Figure 11(a). The SSCs at rising stage and falling stage for Tabatinga.

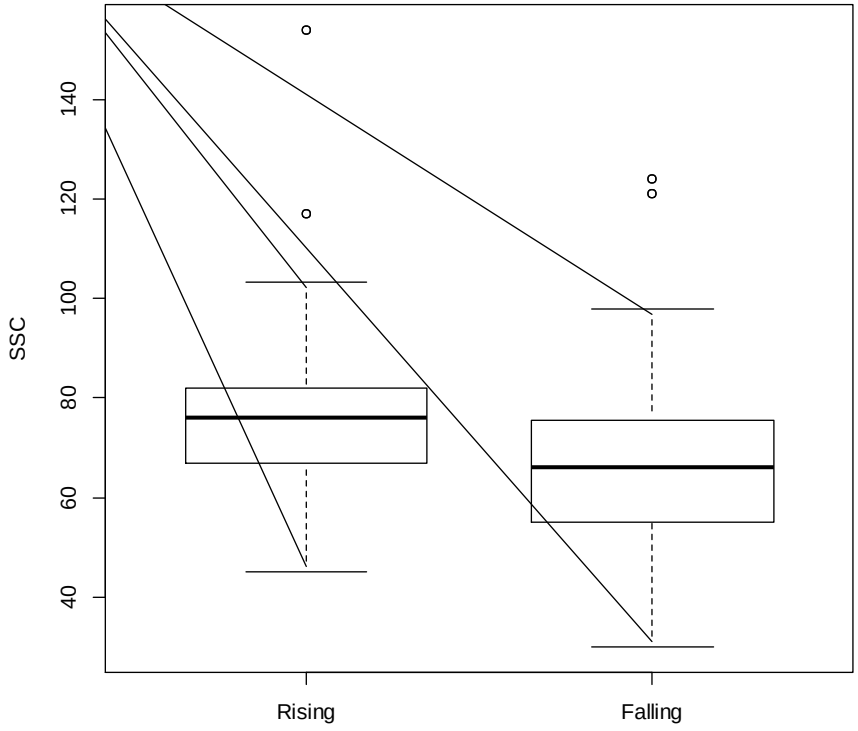

Figure 11(b). The SSCs at rising stage and falling stage for Manacapuru.

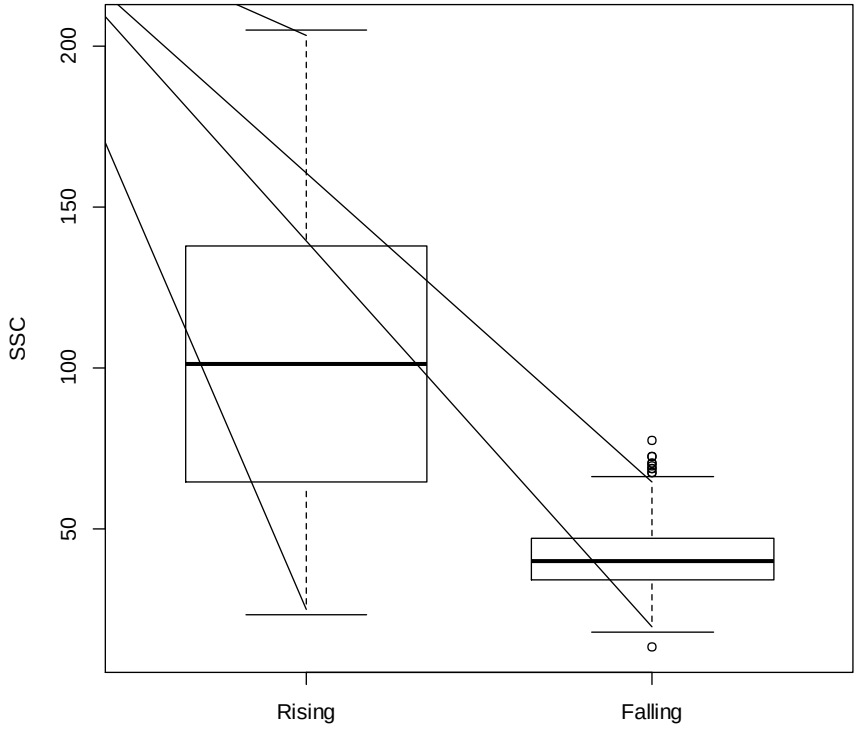

Figure 11(c). The SSCs at rising stage and falling stage for Obidos.

Given that the effect of the hydrological cycle on SSC is evident, the following step should be examining the effect of hydrological cycle on the relationship between REF and SSC. Accordingly, I generated two separate regressions for each region based on the hydrological cycle (i.e., Rising stage and falling stage for Tabatinga; Manacapuru; Obidos (Fig. 12(a), 12(b) and 12(c))). Then, I performed the statistical comparison of two

regressions depending on different hydrological periods. Dissimilar outcomes were observed from different regions.

After the ANCOVA testing concerning different hydrological cycles in Tabatinga, it resulted that hydrological cycles do not affect the SSC or REF (Table 8) while the effect of interaction between SSC and hydrological cycle was shown to be slightly significant ($p = 0.0193$). In order to evaluate the significance of the interaction, more parsimonious modeling after removal of the interaction term was compared with the result in Table 8. ANOVA testing result showed significant difference between the two models ($p = 0.01928$) suggesting that the interaction term is not negligible. Consequently, slopes of regression models of rising and falling stages in Tabatinga are too significantly different to be integrated.

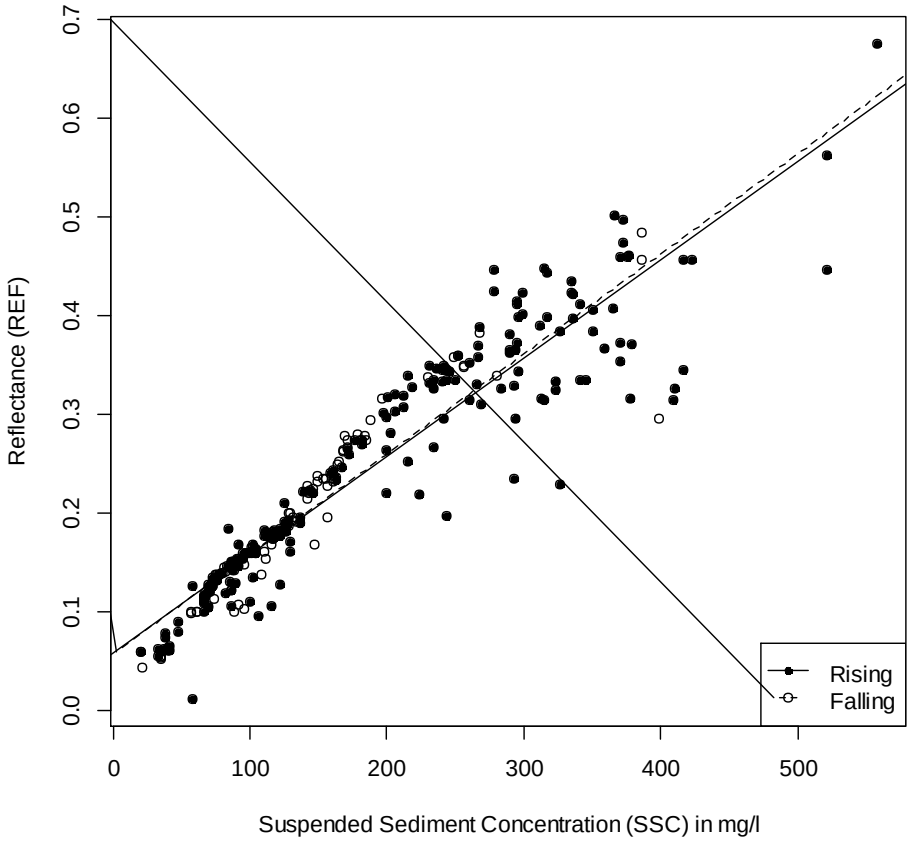

Figure 12(a). The regression between SSC and REF for Tabatinga depending on the hydrological cycle. Regression equation for the rising and falling stage is y = 0.001 + 0.0587 (R^2 = 0.878) and y = 0.00101 + 0.05699 (R^2 = 0.881), respectively.

	Df	Sum Sq	Mean Sq	F value	Pr(>F)
SSC	1	3.475	3.475	2155.793	<2e-16
cycle	1	0.002	0.002	1.082	0.2992
SSC:cycle	1	0.009	0.009	5.539	0.0193

Table 8. The ANCOVA result for comparison between two regressions in Fig. 11(a).

Similar results were retrieved from Manacapuru and Obidos. As expected, hydrological cycles have significant effect on both SSC and REF and the effects of SSC on REF depending on cycles are demonstrated as not necessary to be considered (Table 9(a), Table 10(a)). That is, the slopes of regression models of rising and falling stages are not significantly different and this suggests that the changing aspects of REF value due to SSC level are similar. Given that two regressions have comparable slopes both within Manacapuru and Obidos regions, ANOVA testing was performed to compare y-intercepts for both regression models in order to assess the relevancy of integrating two linear models. (Table 9(b), Table 10(b)). According to the results shown in Table 9(b) and Table 10(b), y-intercepts for both regressions at Manacapuru and Obidos are substantially different. However, the observed errors for y-intercepts were less than 10 mg/l for both stations, which are within allowable, limit in this study, despite statistical significances were displayed. Thus, the blend of regression models from rising and falling stages could be rationalized and I concluded that the regression relationships between SSC and REF seem not to be affected by the hydrological cycles in Manacapuru and Obidos region.

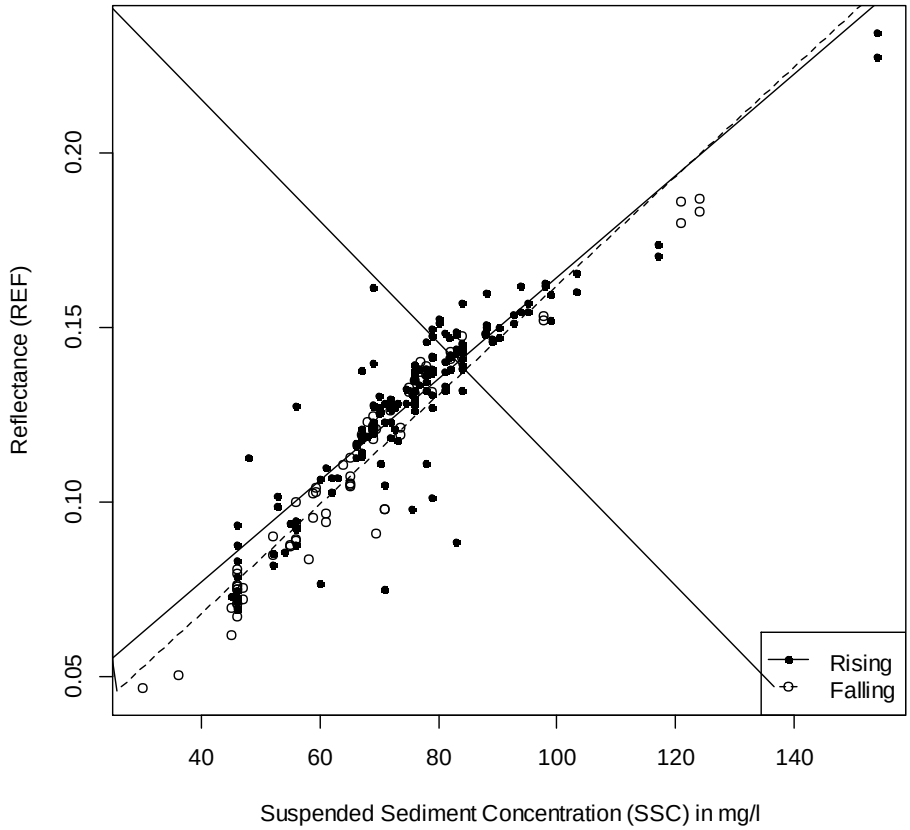

Figure 12(b). The regression between SSC and REF for Manacapuru depending on the hydrological cycle. Regression equation for the rising and falling stage is y = 0.00145 + 0.01875 (R^2 = 0.823) and y = 0.0.00157 + 0.00534 (R^2 = 0.881), respectively.

	Df	Sum Sq	Mean Sq	F value	Pr(>F)
SSC	1	0.17162	0.17162	1619.176	< 2e-16
cycle	1	0.00154	0.00154	14.482	0.00018
SSC:cycle	1	0.0002	0.0002	1.928	0.16624

Table 9(a). The ANCOVA result for comparison between two regressions' slopes in Fig. 11(b).

	Df	Sum Sq	Mean Sq	F value	Pr(>F)
SSC	1	0.17162	0.17162	1612.88	< 2e-16
cycle	1	0.00154	0.00154	14.43	0.000185

Table 9(b). The ANCOVA result for comparison between two regressions' y-intercepts in Fig. 11(b).

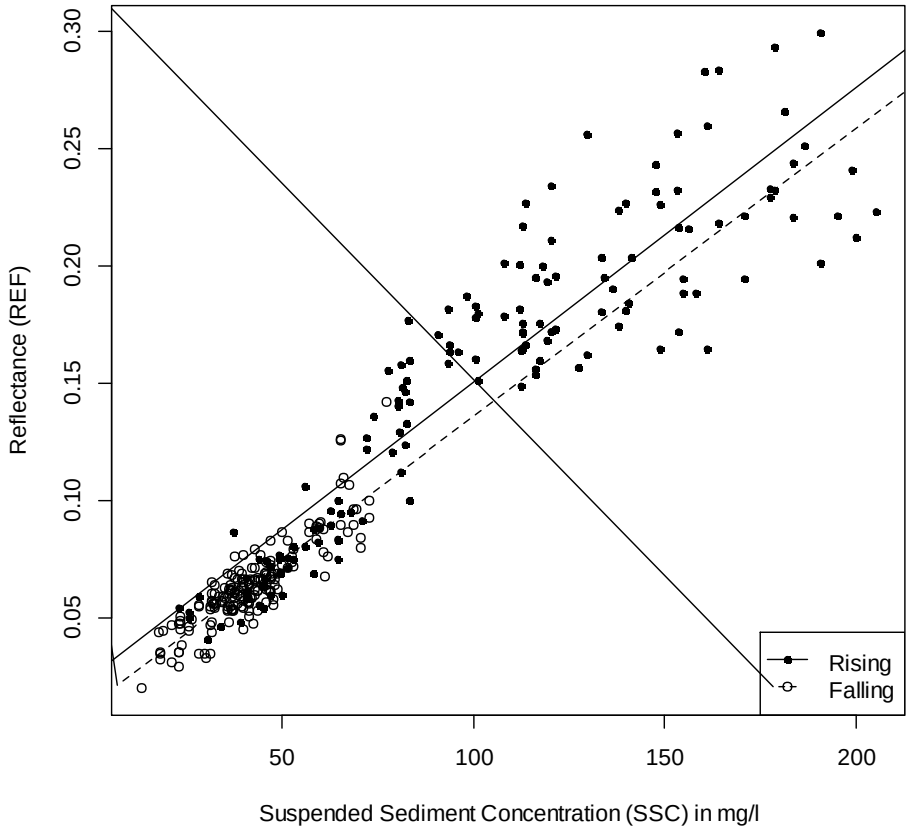

Figure 12(c). The regression between SSC and REF for Obidos depending on the hydrological cycle. Regression equation for the rising and falling stage is y = 0.00125 + 0.0251 (R^2 = 0.825) and y = 0.00123 + 0.0131 (R^2 = 0.76), respectively.

	Df	Sum Sq	Mean Sq	F value	Pr(>F)
SSC	1	1.2077	1.2077	3231.239	< 2e-16
cycle	1	0.0075	0.0075	20.018	1.07E-05
SSC:cycle	1	0	0	0.049	0.824

Table 10(a). The ANCOVA result for comparison between two regressions' slopes in Fig. 11(c).

	Df	Sum Sq	Mean Sq	F value	Pr(>F)
SSC	1	1.2077	1.2077	3240.84	< 2e-16
cycle	1	0.0075	0.0075	20.08	1.04E-05

Table 10(b). The ANCOVA result for comparison between two regressions' y-intercepts in Fig. 11(c).

Consequently, models were statistically proven to be different depending on hydrological cycles in Tabatinga, which is the most upper reach of the Amazon River. The statistical test failed to confirm the difference of REF values based on SSC depending on hydrological cycles in Manacapuru and Obidos, which are mid- and lower reaches, respectively. However, the significance of statistical testing in Tabatinga does not manifest that segmenting the regression model based on hydrological cycle is an ideal way based on the true association between SSC and REF. This observed significance could be simply due to the higher variations of REF in high SSC range, which is mostly during the rising water period.

Also in Manacapuru and Obidos, although the testing result suggests the unlikeliness of observing two distinct rising and falling data from an identical regression model in each region, the distinct patterns of REF behavior based on SSC depending on hydrological cycle is hardly observed. In addition, substantial differences in SSC ranges of different hydrological cycles in both regions leave a large space for uncertain inferences of the model in an uncommon range. Therefore, hydrological cycles within a

year should not be regarded as fundamental way of segmenting regression models taking the characteristics of SSC and levels of REF's reactivity into account.

Individual modeling

Different testing results based on hydrological cycles (Table 8, 9(a), 10(a)) imply different associations of REF and SSC. As of yet, studies on seasonal or regional variations of relationship between REF and SSC have not been seriously performed within a large basin though Mertes et al. (1993) has offered an implication about this. According to Mertes et al (1993), the rate of scattering and backscattering of suspended particles is predominantly affected by mineralogical and textural characteristics, and sediment color, type, size also significantly affect the ranges of reflectance. Though located in the same basin, the regression models retrieved from three distant regions (approximately 1,000 km from Tabatinga to Manacapuru and 600 km from Manacapuru to Obidos) are affected by their own particular discharge rates, velocity, precipitation, wind, turbidity, tributary structures, bathymetry, vegetation, and soil properties. Since reflectance recorded in remotely sensed data is determined from complex mixture of these multiple factors, seasonal and regional dependency of models could not be described in a single context (e.g. hydrological cycle). Hence, individual modeling depending on time and space is desirable and these models will effectively guide the analysis of the geo-environmental characteristics that affect the models.

In Tabatinga, correlation of SSC with REF tends to be high in low SSC range and correlation gradually drops as SSC increases (Fig. 6(a)). Taking notice of this distinct feature, I tried to segment regression models using the software SegReg. SegReg

introduces the breakpoint of an independent variable in a regression model based on the maximization of the coefficient of determination and performing the test of significance (Oosterbaan, 2009). As a result, one breakpoint was suggested around SSC value 200 (mg/l), which agreed with the value obtained through visual inspection. Given this finding, correlation of SSC with REF in the range below 200 (mg/l) is significantly high (R^2=0.91) and sufficient for individual modeling, but further examination was thought to be necessary only for SSC ranges above 200 (mg/l) where they tend to have high variations. In order to investigate the patterns of REF response based on SSC over 200 mg/l, 11 years of samples were plotted for each month to carry out a thorough inspection of the model (Fig. 13). An interesting pattern was observed that, for samples from March to April, a conspicuously lower REF response to the same SSC value was recorded, a period which matches with the falling stage of SSC within a year (Fig. 13). In addition, a logarithmic model was suggested for that particular period during which the REF response shows a tendency to saturate as SSC value increases. When those samples from that particular period (March to April) were separated from the entire model, the association between SSC and REF for the remaining months (i.e. May to February in following year) showed a closer linear pattern (R^2=0.93). This seasonal variation of REF response has been introduced in Madeira River (Villar et al., 2012) but not in the mainstream of Amazon River (including Solimoes River). Thus, two different regression models depending on two distinct periods within a year were suggested for Tabatinga. (Table 11): first regression model by samples from May to following year's February

and; second regression model by samples from March to April (when SSC is falling during a year).

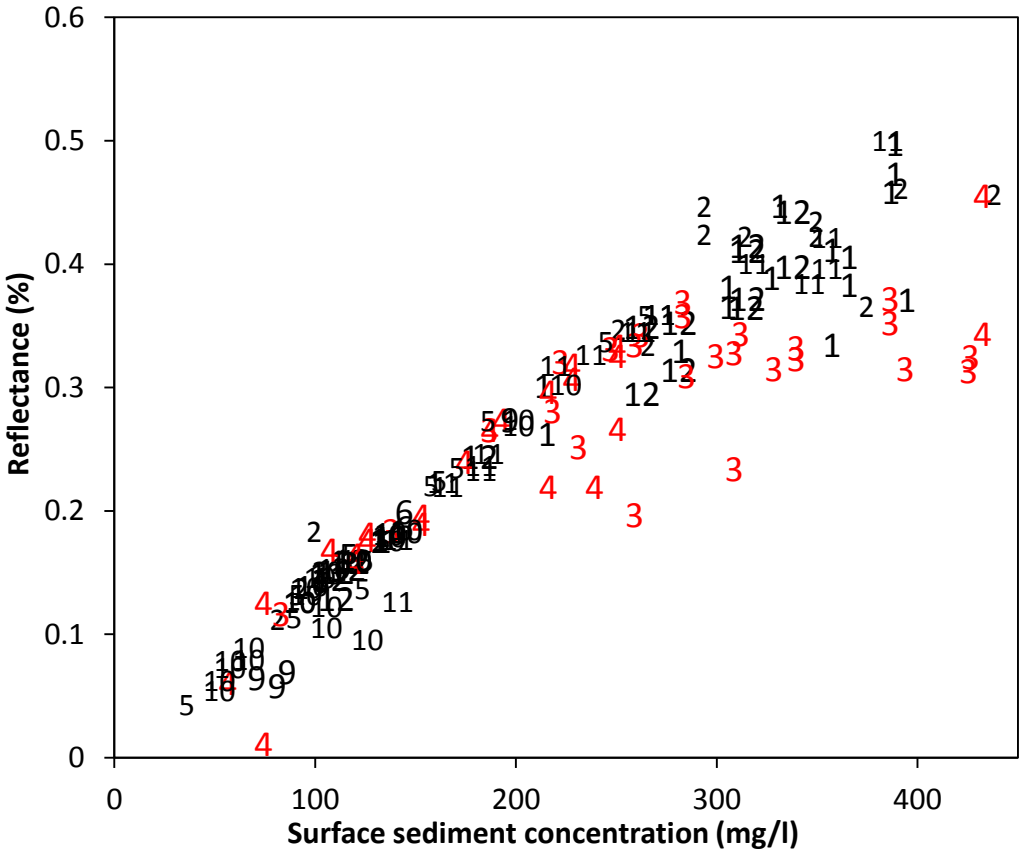

Figure13. Monthly plotted scatter plot for Tabatinga suggesting two regression models.

Manacapuru has the smallest ranges of both SSC and REF (Fig. 8(a), (b)); and has substantially high correlation between REF and SSC throughout the entire SSC range. However, slightly inconstant variations of the residuals along the regression line are observed (Fig. 7(b)), suggesting heteroskedasticity-robust regression modeling for this

site (White, 1980). Coefficients and the root mean square error retrieved in this study are reported in Table 11.

At Obidos, REF variations across the entire SSC range is obviously not constant (Fig. 15), and this fact suggests the necessity of segmentation of the model. To obtain clues about portioning the model, models were first compared depending on its hydrological cycle, and it is considered not a clear criterion[11].

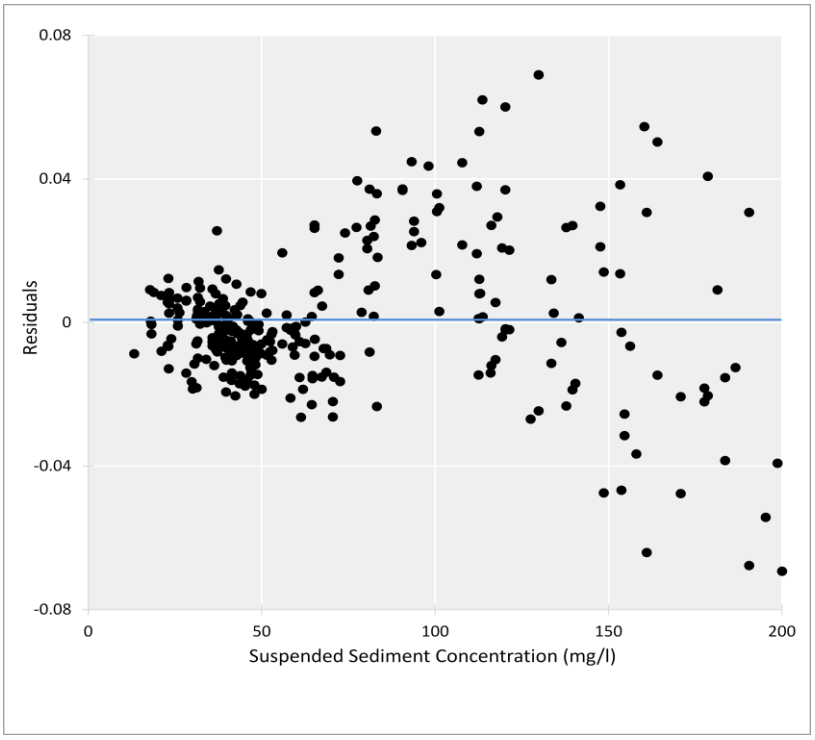

Figure 14. Linear regression residual plot for Obidos.

Hence, two residual plots were examined, with one plotted against time to see the existence of temporal autocorrelation in association between REF and SSC within a year rather than the hydrological cycle, and the other against SSC values. Though temporal

[11] Even with such a high p-value (p=0.824, Table 10(a)), significantly different SSC ranges of rising and falling water cycle (p=2e-9) inheres critical uncertainty outside the observed SSC ranges.

autocorrelation in the time-series residual plot was expected due to the seasonal dependency of SSC and REF, no clear pattern was observed. However, a clear pattern was observed in the residual plot against SSC values (Fig. 14), suggesting that it is more relevant to segment the model based on the SSC values. Since residuals throughout SSC are not constant, different characteristics of REF and SSC associations were suggested for each segment, regardless of statistical significance between regression segments.

Two segments were arbitrarily proposed based solely based on the values of SSC. The first segment up to 75 mg/l SSC showed considerably high correlation (R^2=0.73) and statistical testing over samples below 75 mg/l depending on hydrological cycle resulted in a considerably high p-value (0.97). In addition, around 63% (130 out of 207) of samples from discharge-fall period was included in this segment, suggesting no clear evidence to segment regression model temporally. The second segment was constructed with remaining samples with SSC range above 75 mg/l. Most of the samples constituting the second segment came from the rising stage of hydrological cycle and the second segment showed lower correlation (R^2=0.63) than the first segment. A clue has been provided that in Madeira River, the response of reflectance could have variations depending on sediment concentration cycle within the rising stage of the water (Villar et al, 2012). However, rising and falling SSC periods are randomly mingled that it is difficult to find out any patterns of samples' distribution through visual inspection. While the statistical testing over different regression models from rising and falling SSC periods indicated significant differences (p=0.014), the correlation (R) decreases below 0.4 for both regression models from rising and falling SSC periods, significantly dropping the

reliability of models. Therefore, I decided to accept slightly higher noise for the second segment than the first segment. In order to take non-inconstant variations of residuals for segmented models, robust standard errors were generated to estimate SSC by using REF in Obidos (Table 11).

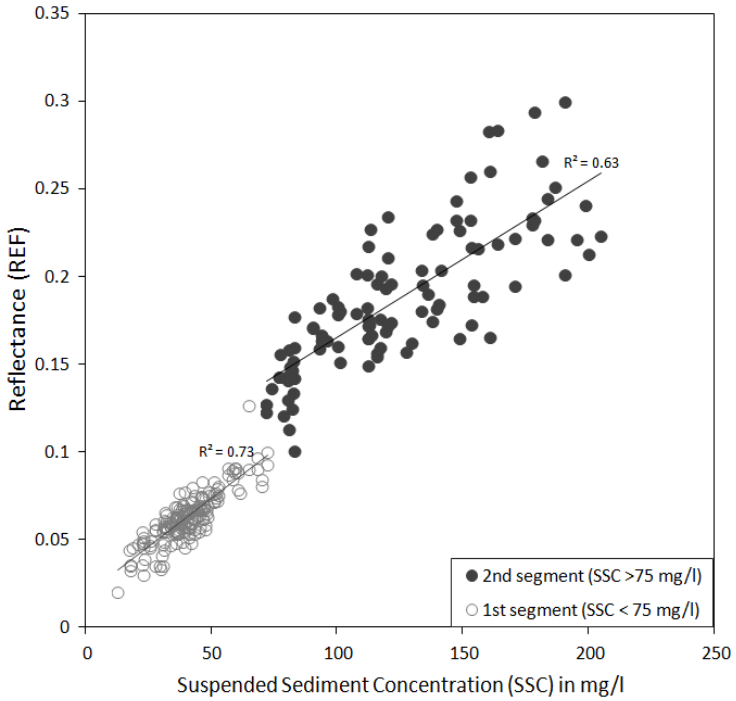

Figure 15. Multi-regression model in Obidos

Model	Tabatinga		Manacapuru	Obidos
Coefficient	Jun-Feb (following)	Mar-May		
Regression Model	Linear	Logarithmic	Linear	Multiple
β_0	909.1 (0.91)	-0.4848 (0.02)	4.731 (2.93)	-4.1994 (2.01)
β_1	-49.54 (24.32)	0.1421 (0.01)	554.197 (25.04)	1.5772 (0.01)
β_2	0		0	691.598 (8.93)
R^2	0.92	0.85	0.86	0.73
RMSE (mg/l)	29.31	35.47	6.15	6.5
n	135	72	232	313

Table 11. Summary of coefficients and Root Mean Square Error (RMSE) of models retrieved from each site. Model follows regression function, $SSC = \beta_0 + \beta_1 \cdot REF + \beta_2 \cdot X$ or $SSC = \beta_0 + \beta_1 \cdot \ln(REF)$. Number in parenthesis () after each coefficient indicates robust standard error.

3.2 GENERATION AND ANALYSIS OF RESULTS THROUGH SSC DISTRIBUTION MAPS

Representation of the results is one of the key parts toward the goal (analysis of mega-pattern SSC distribution) of this study. Through visualization of time-series surface sediment maps, it becomes possible to monitor the dynamic patterns of surface sediments' distribution, which allows for investigating sediment transport in the main channel, interactions with its floodplain, and flow into the main channel from different tributaries. Effective visualization through multi-temporal mapping enables exploration of more meaningful SSC patterns in larger scale taking floodplains and tributaries into account, enhancing the decision-making processes in various applications regarding fluvial environments. SSC maps are generated by applying retrieved calibration model (section 3.1.4) to qualified MODIS time series images (MOD/MYD09Q1).

Interpolation of missing pixels

Before applying calibration model to qualified MODIS time series images (MOD/MYD09Q1), unqualified pixels (i.e. pixels without data) should be estimated to generate continuous surface sediment concentration maps. After the thorough winnowing out of pixels through QA and SZA assessment, only qualified pixels were left. On the other hand, this process produced approximately the same quantity of empty spaces in images as number of filtered out pixels. Hence, I decided to predict values of empty cells on the water surface using interpolation techniques. Estimation of cells without values is considered relevant for the following three reasons. First, the pattern of spatial

autocorrelation of SSC is significantly high in main channel of Amazon River (Fillizola et al., 2009). Secondly, pixels to be used as input data for interpolation is considerably richer in both quality and quantity than the pixels to be predicted. Lastly, pixels to be interpolated are not concentrated in certain area, but instead show a random scattering pattern.

To fill missing pixels within the water body, the Local Polynomial Interpolation (LPI) was utilized based on values of existing nearby cells. LPI is a widely used interpolation technique when there are short ranges of variations in the surface. Unlike Global Polynomial Interpolation (GPI), LPI fits different polynomial functions for each of the smaller sub-regions. In the Amazon River's mainstream, slowly varying SSC over a long range is a general trend (Fillizola et al., 2009); however, due to the effects from tributaries where they have distinct SSC characteristics from mainstream of Amazon River (i.e. Negro, Madeira, Tapajos), short range variations should be considered in addition to long range variation. Therefore, the LPI method is thought to be appropriate for taking into a slowly varying surface over a long range while still capturing local variations[12].

The complete water extent should be defined in order to restrict the extent of the water body in the interpolation process, and MODIS MOD13Q1 products were supplemented to retrieve the complete water body extent. MOD13Q1 is a 16-day

[12] Compared to Kriging method, LPI does not give information about predicted error. However, in this study, I needed one predicted value for each cell and my objective was to examine spatial pattern of SSC distribution rather than precise estimation (calibration) of SSC value for each cell. In addition, LPI is more efficient than Kriging in terms of intensity of computation, considering over 1,000 images needed to be processed.

composite product containing various layers including red (MODIS band 1), NIR (MODIS band 2), blue (MODIS band 3), NDVI and EVI at a 250 meter spatial resolution, which is designed to provide consistent conditions about water and vegetation property. For two primary reasons, the 16-day composite product was considered to be appropriate in retrieving water extent. First, geomorphologic processes in the Amazon River body is noticeably slow. Accounting for the fact that the possible maximum difference in days between the day of pixel scanning the surface and the day of event happening on the surface is at most 16 days, the chance of 250 meter resolution pixels to shift to another class (from water to other class or from other class to water) in this short period is very small. Secondly, the 8-day composite products (MOD/MYD09Q1) still often have fairly amount of cloudy pixels in some regions, which affect the correct delineation of the channel body, especially during the wet season. However, there are scarcely any cloudy pixels around main channel of the river in MOD13Q1 product, allowing for the correct extraction of the water body.

An Unsupervised Iterative Self-Organizing Data Analysis (ISODATA) classification method was used to extract water extent from 3 layers (MODIS band 1, band 2, band 3) in MOD13Q1. Thirty classes were defined for the classification and convergence threshold was set to 95 %. After obtaining the water extent from ISODATA classification for every 16 days, qualified 8-day composite reflectance pixels from MOD/MYD09Q1 were inserted into the water mask (This process was performed in Python, see appendix).

Representing results through SSC maps

SSC maps were generated by applying calibrated models between 11 years of SSC and REF data from each region to the MODIS images retrieved in the previous section (3.2.1). For this step, variables (SSC and REF) were switched from the retrieved models to invert the models for each region (Table 11), since the SSC value for sites that have not been sampled should be estimated from the REF value recorded in MODIS image. Since three to four images were possible to retrieve every month from 2000 to the present time, I decided to show SSC maps only for one representative year 2007, due to lack of space in this thesis. The year 2007 is considered to be representative, because the Amazon River's hydrological behavior is normal in this period (i.e. mean monthly discharge corresponds to those of 11 years' average) without severe events (i.e. flood or draught) and datasets for SSC and REF are relatively evenly distributed throughout the whole year.

Once SSC maps were retrieved, proper color scheme with consideration given to image enhancement (in order to present more contrast between similar SSC values) is generated and applied to images in order to compare SSC maps visually, since the whole SSC range (and also concentrated SSC range) is different depending on periods within a year even for the same region (extent). To present SSC rates quantitatively, classified color scheme was chosen with 10 mg/l interval for Manacapuru and Obidos, where they have relatively small SSC ranges; while 30 mg/l interval was chosen for Tabatinga, where SSC range is large (Fig. 7), while also taking into account of the root mean square error (RMSE) of each regression model (Table 11). Color Brewer 2.0 (http://colorbrewer2.org/) and Color Scheme Designer (http://colorschemedesigner.com/)

were referred when creating sequential color ramp. Figures 16, 17, and 18 are estimated SSC maps in 2007 for Tabatinga, Manacapuru and Obidos, respectively.

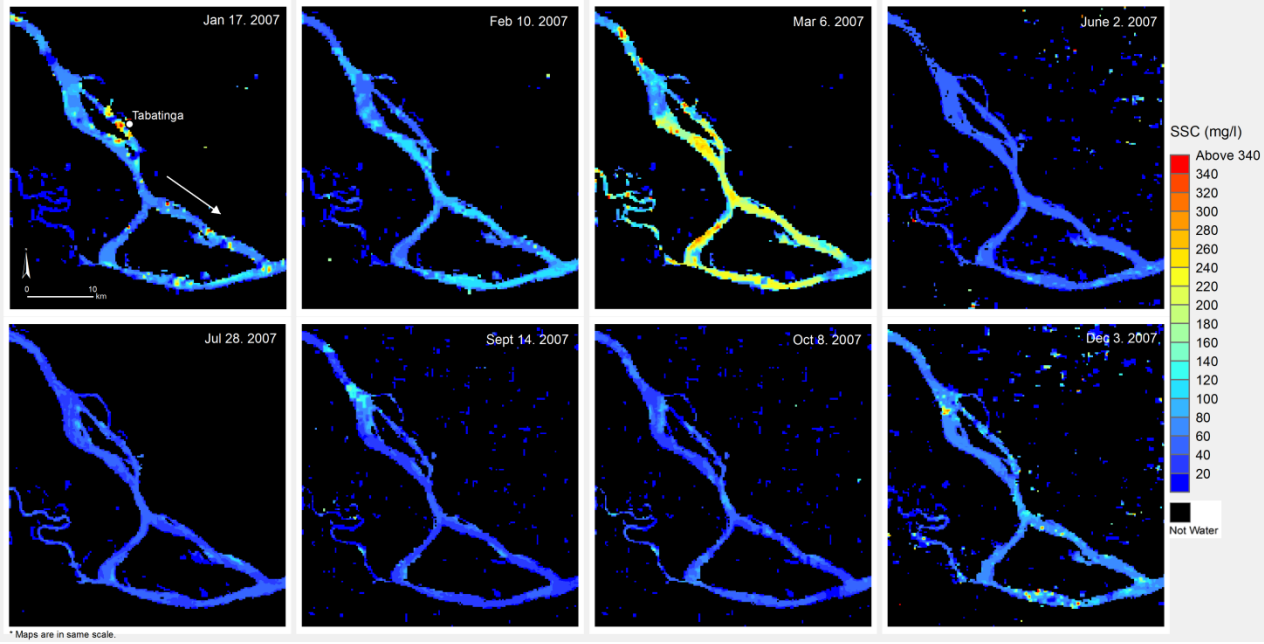

Figure 16. SSC maps for Tabatinga in 2007.

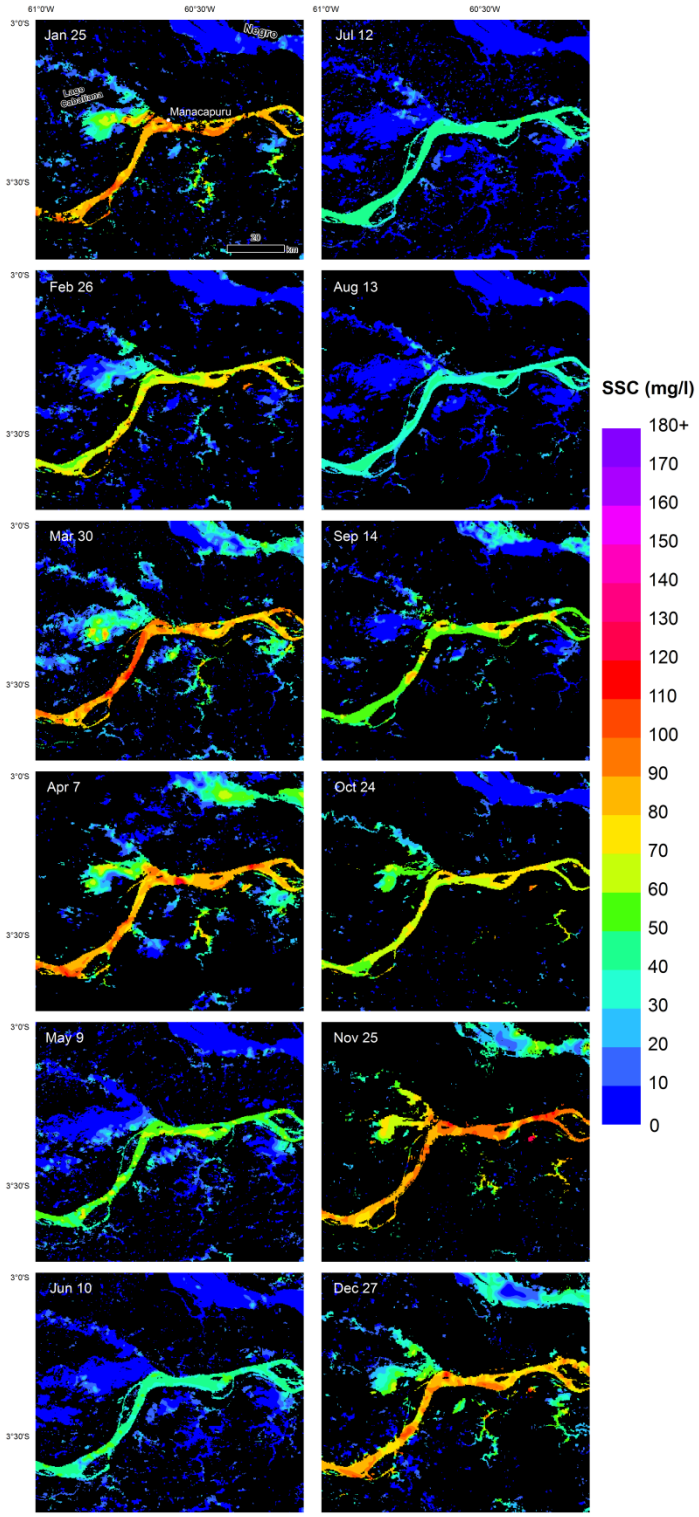

Figure 17 (a). Whole year (2007) SSC maps in Manacapuru. One image from each month is displayed within a two week interval.

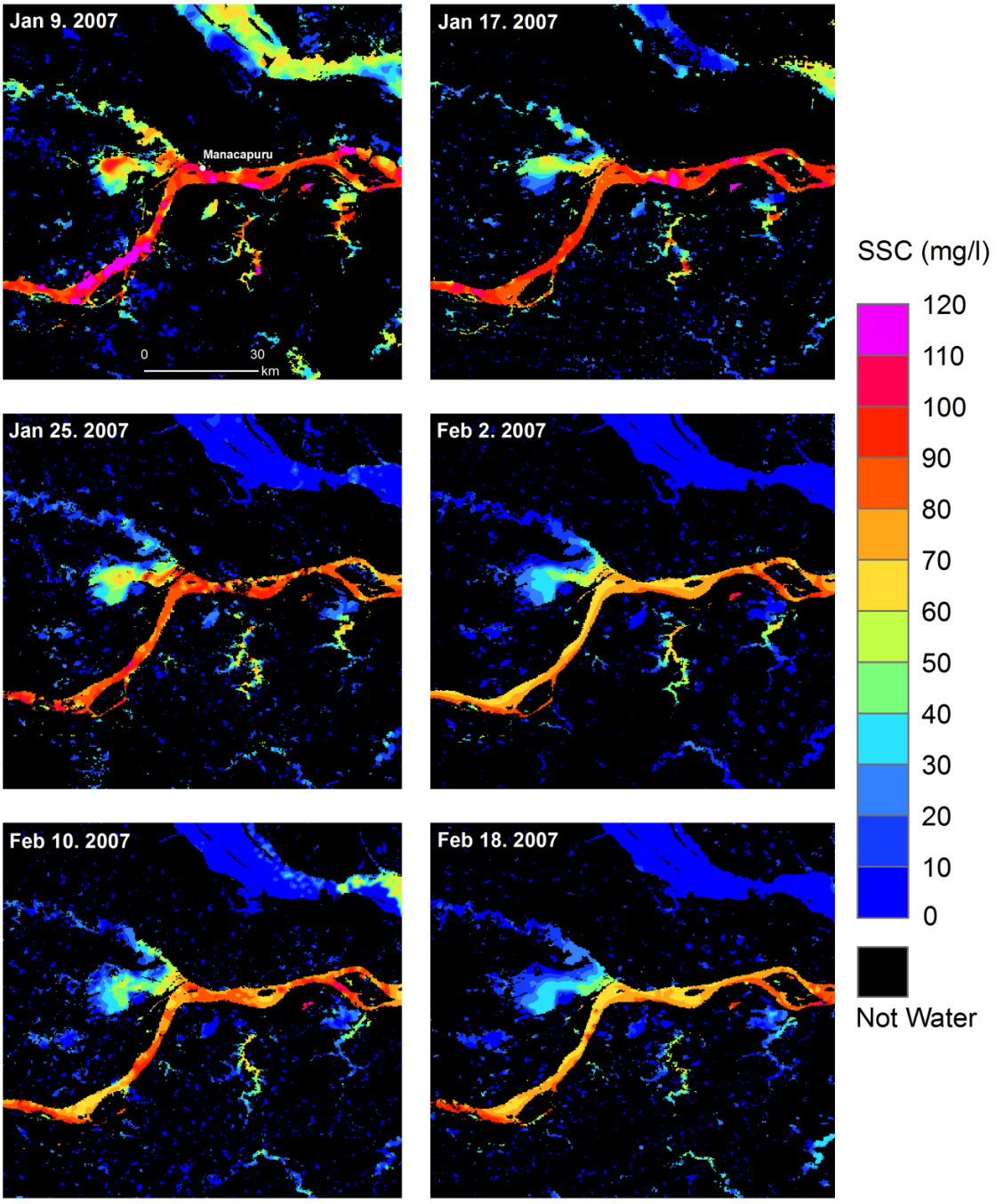

Figure 17 (b). SSC maps for Manacapuru in early 2007. These maps are provided to show capability of technique implemented in this study capturing SSC dynamics during short period of time scale.

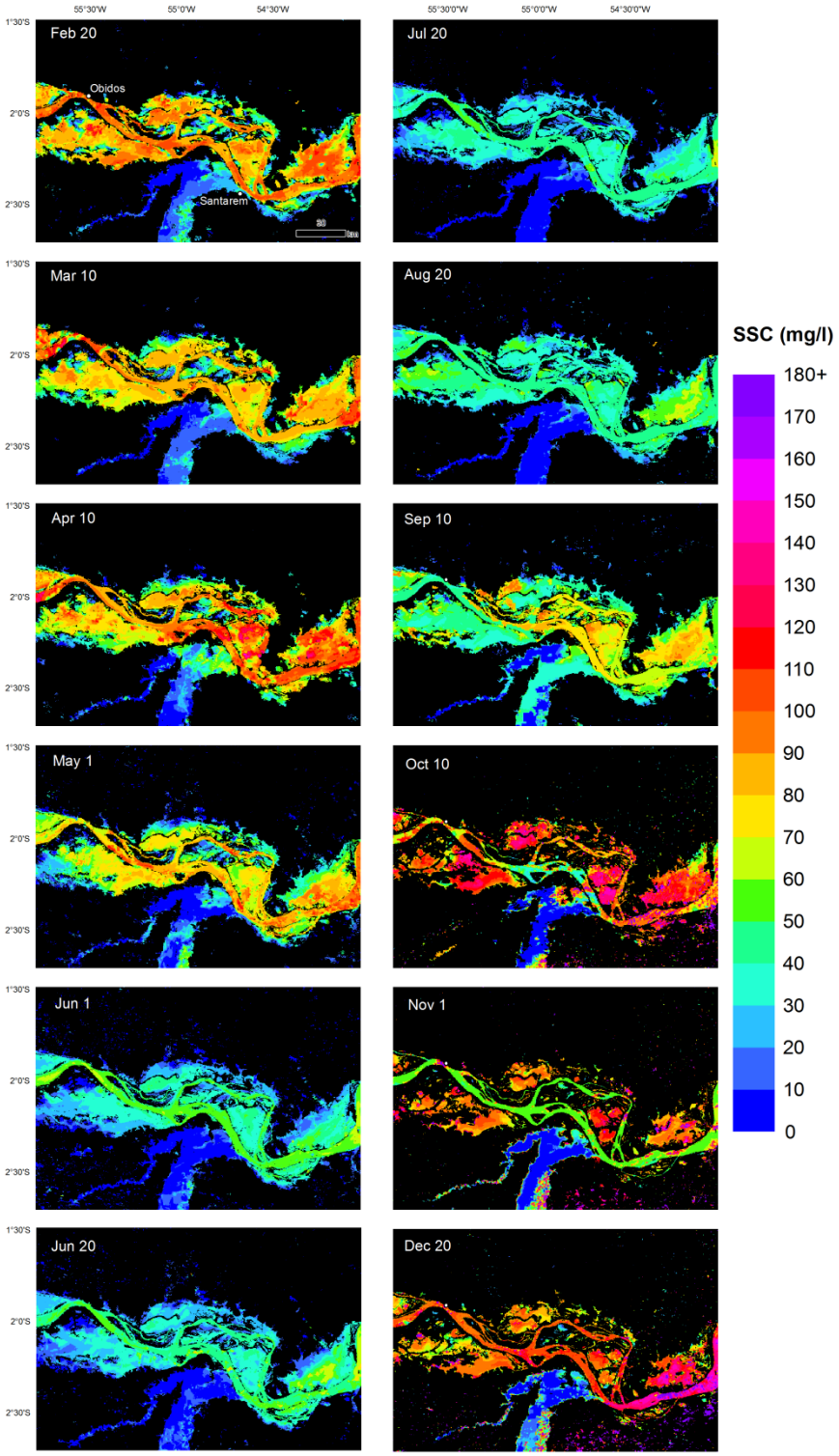

Figure 18 (a). Whole year (2007) SSC maps for Obidos. Only few are demonstrated (approximately one for each month) due to space limitation.

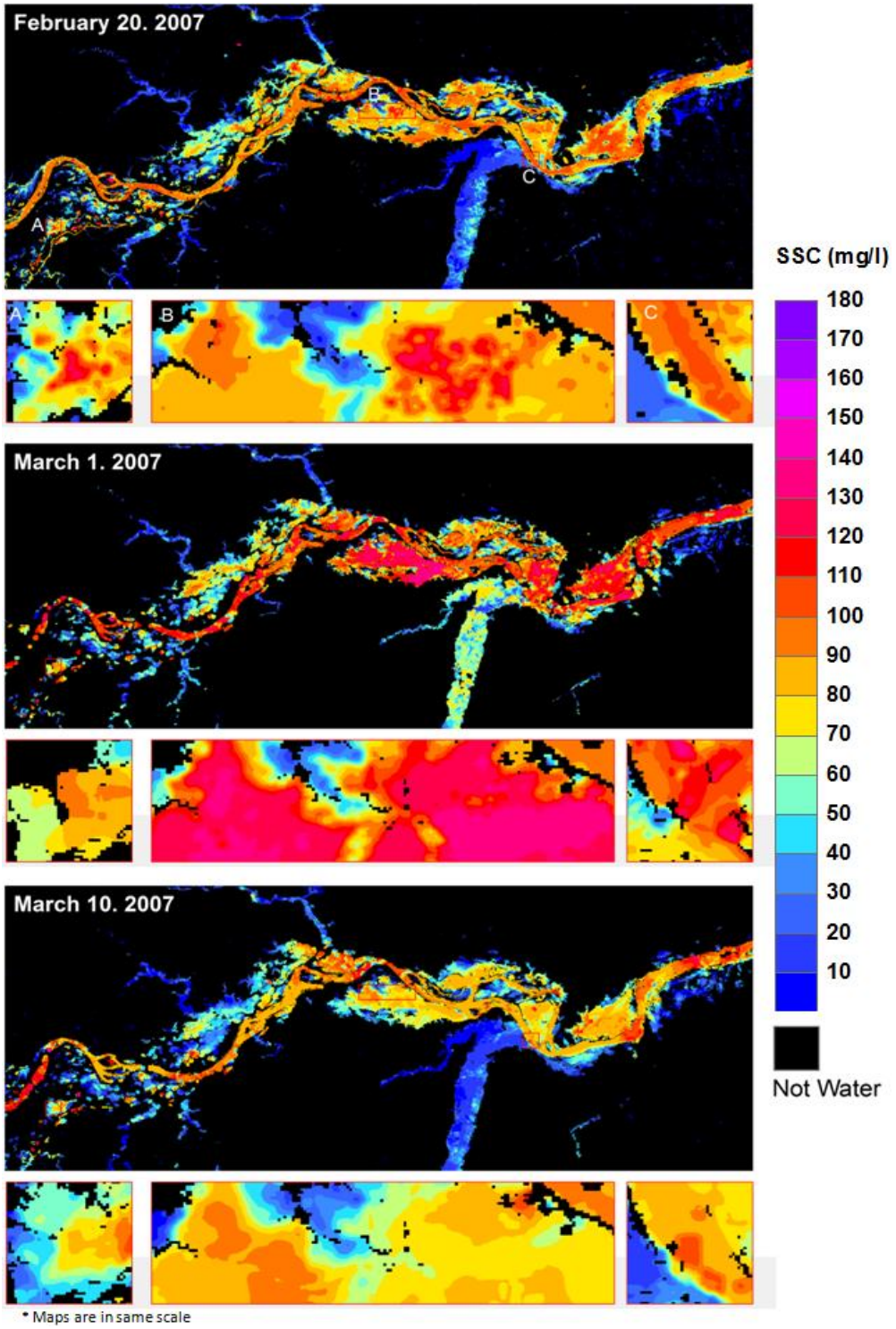

Figure 18 (b). SSC maps for Obidos in early 2007. These maps are provided to show capability of technique implemented in this study capturing SSC dynamics during short period of time scale. Inset maps are magnified from extent indicated by red rectangles. Images in inset maps are resampled to 50 meter resolution for visualization purpose.

Analysis of surface sediment distribution patterns through SSC maps, Case of Obidos in 2007

In this section, an example of effective monitoring of surface sediment distributions in two distinct periods (i.e. falling water stage (A) and rising water stage (B)) in 2007 around Obidos is demonstrated. Around Obidos, complex floodplains are associated with Amazon River mainstream and tributaries, representing downstream characteristics of the Amazon River (Hess et al., 2003; Sippel et al., 1992; Dunne et al., 1998; Bonnet et al., 2008). Extensive lakes in this region are mainly formed by vertical accretion and flood dynamics in the anabranching main channel (Fig. 19 (A), Latrubesse 2012). Figure 19 shows both the surface sediment concentration maps during falling (A) and rising (B) water stages in 2007.

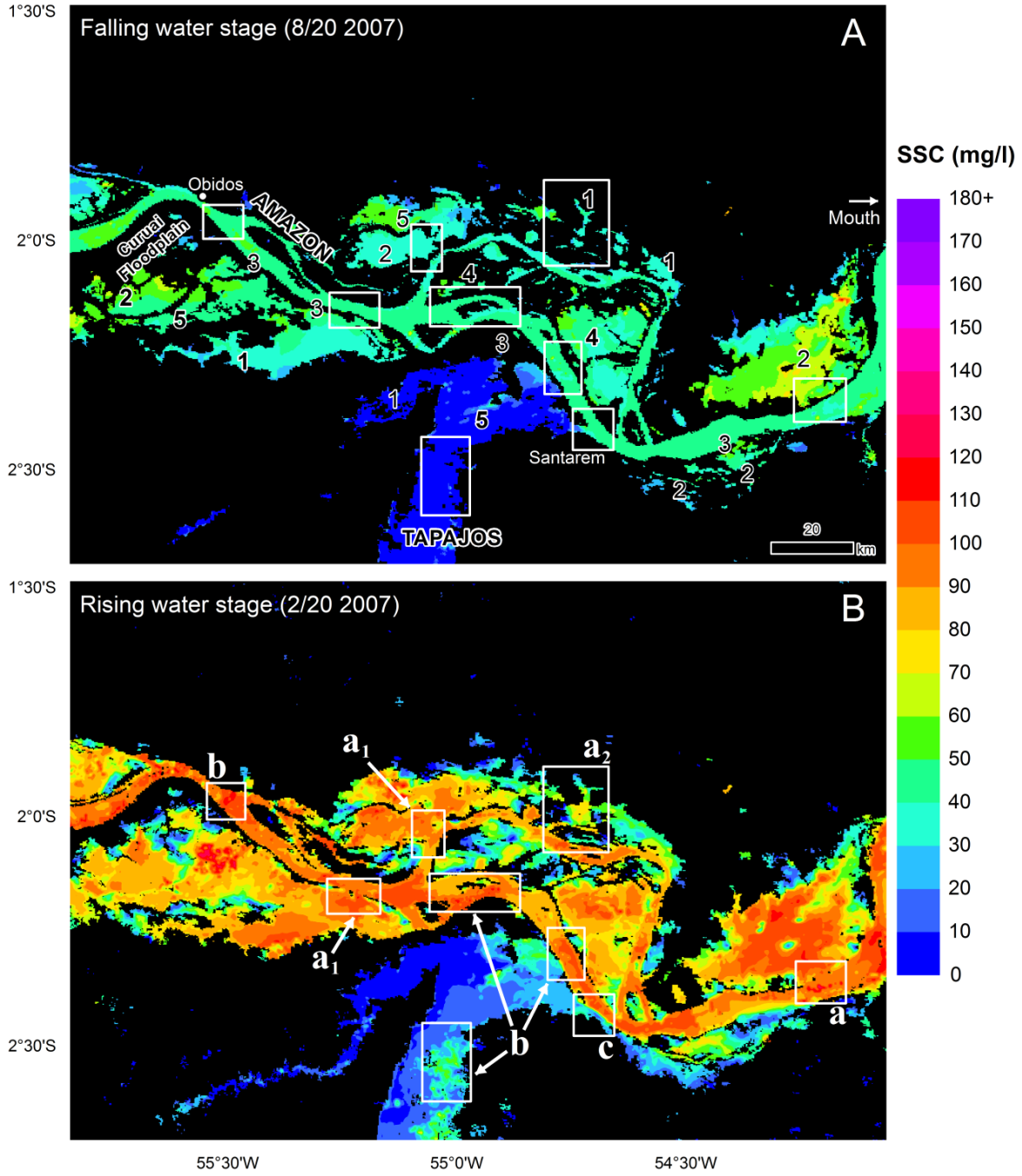

Figure 19. Comparison of surface sediment concentration maps during falling (A) and rising (B) water stages in 2007 around Obidos. Lakes categorized in falling water stage map (A) follows the category by Latrubesse, 2012: blocked valleys (1), rounded lakes in a drainage floodplain (2), spectacular levees confining the river flow along a narrow corridor inside a water saturated floodplain (3), large islands and island lakes (4), and delta systems entering in the floodplain lakes (5). Spatially linked rectangles (white) indicate representative regions where objectives of the study are demonstrated. Note that most of the levees confining the floodplain lakes are thinned or flooded during the wet season.

The regions overlaid with spatially-linked white rectangles in both images in Figure 19 show representative cases, where the surface sediment concentration maps successfully display the variability of spatial and temporal distribution patterns of SSC. One of the most remarkable phenomena observed is the capture of interactions between the channel and the floodplain (**a**). In the rising water period (B), it is readily detectable that surface sediment in the main channel flood over to floodplain lakes that are confined by levees during the low water season (A). Note the link from mainstream to Curuai floodplain lake generated by flood in mainstream ($\mathbf{a_1}$) in relation to fact that around 80% of total water input into the this floodplain is constituted by the mainstream (Bonnet et al., 2008) and sediment from the main channel takes up nearly 50% of the annual sediment flux entering to the floodplain (about $710 \cdot 10^3$ t/yr, Bourgoin et al., 2007). Monitoring spatial and temporal patterns of sediment is significant, since during the storage of water in the floodplain, biogeochemical alterations take place, which are affected by the spatial and temporal patterns of local hydrology (Mertes et al., 1995). Another interesting pattern observed is connection of lakes that are blocked valleys in water falling periods ($\mathbf{a_2}$) from the branch of mainstream by floods.

Distribution patterns of surface sediment concentration along the channel are also successfully shown (**b**)[13]. The tendency of higher SSC along the middle of the main channel and east bank in Tapajos River is observed. Examination of the spatial variability of SSC along the channel allows the analysis of sediment transport pattern in

[13] Obviousness decreased in this case, because I adapted 10 mg/l interval classified color ramp to represent SSC; however, when continuous (stretched) color adapted, spatial distribution of SSC becomes more obvious.

anabranching system (Latrubesse, 2008) and identification of local geomorphic features (Filizola et al., 2009). The impact of tributaries to the main channel is explicitly shown through the floodplain delta system in Tapajos River, the largest clear water body in the world (**c**). At the confluence, most of Tapajos River delta system is still suffering from stable levee complex built by the Amazon River's main channel and allows only a narrow connection to the mainstream (Latrubesse, 2012). Flowing out from this small mouth, sediments from Tapajos River are not substantially mixed with sediments in the mainstream and flow into the rounded lakes in the drainage floodplain along the main channel of Amazon River.

Chapter 4: Discussion

Examining the spatial and temporal surface sediment distributions in rivers is an essential step toward understanding large fluvial systems. Based on this objective, this study focused on recognizing the dynamic patterns of SSC distribution on a multi-temporal scale (different from other studies focused on precise estimation of SSC quantity) and the platform that I constructed through the thesis has well demonstrated its capability (section 3.2). However, due to the uncertainties in nature, existence of variability in regression modeling should be considered. Distinct from other studies performed in the Amazon Basin, one of the noticeable (and unique) efforts made in this study to overcome this challenge is securing the unprecedentedly largest sample size and strict filtrations of them to approximate to the actual parameter. Thus, with a qualified high sample size, it is expected that calibration models implemented in this study is closest to the parameter than other existing models proposed from other studies.

Fundamental uncertainty lies also within remote sensing applications. The launch of earth observing satellites have made data acquisition incredibly simple, enabling performance of research without fieldwork. The remote sensing approach is convenient and efficiently facilitates studies on earth surfaces. However, there are fundamental limitations in this approach that in many cases, without supplement of field data comprehensive understanding about study sites, is challenging. For example, there were no SSC samples available for Manacapuru in 2007; however, it was possible to reconstruct SSC distributions over vast area around Manacapuru and its floodplain lakes

in 2007 entirely with remote sensing images (Fig. 17). Since remote sensing imageries have undergone thorough processing steps, reconstruction from remote sensing data is assumed to provide reliable data. However, in the geomorphic perspective, an unexpected pattern was observed around Manacapuru in 2007 that SSC increased in the main channel again in March (Fig. 17, it gradually decreases normally in all other years), which cannot be explained solely based on remotely sensed imagery. This event could be due to overestimation of remote sensing images, or some extreme event could have occurred in that particular place. Thus, making up for limitations from remote sensing approach is the task for future work.

Conclusion

The capability of the platform (to investigate patterns of surface sediment distribution based on multi-temporal remote sensing data in large fluvial system) introduced in this study is successfully presented in the Amazon River Basin, which is the most complex and largest river system on earth. Upon building the platform, resolutions of MODIS remote sensing data are shown to be sensitive enough to capture the variability of surface sediment and spatial patterns of distribution of surface sediment. Therefore, in addition to the previous works (section 1.2) performed in Amazon River, I provided three major findings through this study: a) higher scale surface sediment variability of channel-floodplain interaction; b) internal variability of surface sediment along the anabranching main channel (and in floodplain lakes); c) influences of tributaries along the Amazon River in mega scale, which are the crucial factors in understanding the morpho-dynamics of the large river system. Also, I was able to prove the d) different nature of association between surface sediment and reflectance depending on time and space in a large river system.

In addition, considering the fact that most of the large rivers on earth are classified as having an anabranching channel pattern (Latrubesse et al, 2008) such as Amazon River, the capability of this platform in characterizing the patterns at a smaller scale to understand the sediment transport in complex and dynamic branches and tributaries' impacts is successfully proven. Thus, a high potential in the application of the platform developed in this study (analysis of surface sediment distribution pattern

through remote sensing technique) over other large river systems in earth is seen. Therefore, this platform will provide other similar studies in different large rivers around the world with the solid framework. Furthermore, this platform is not limited to MODIS but, with implementation of other sensors with varying resolutions, this platform will also work to capture different characteristics depending on its purposes (e.g. smaller scale river, more dynamic patterns, etc). However, regardless of their purposes, it is obvious that efficiently building the surface sediment database based on remote sensing data should be broadly beneficial to various fields concerning fluvial environments.

Since sedimentary process is the basis for understanding morpho-dynamics in a large river system, an easier way of monitoring sediment concentration and its complex distributions into the multichannel system and through the floodplain as proposed in this work is expected to be instrumental in support of studies on large river system and fluvial ecology, in which distribution of sediment concentration works as a key variable in system function.

Appendices

Appendix 1. Image processing flow implemented in ArcGIS 10 Model Builder.

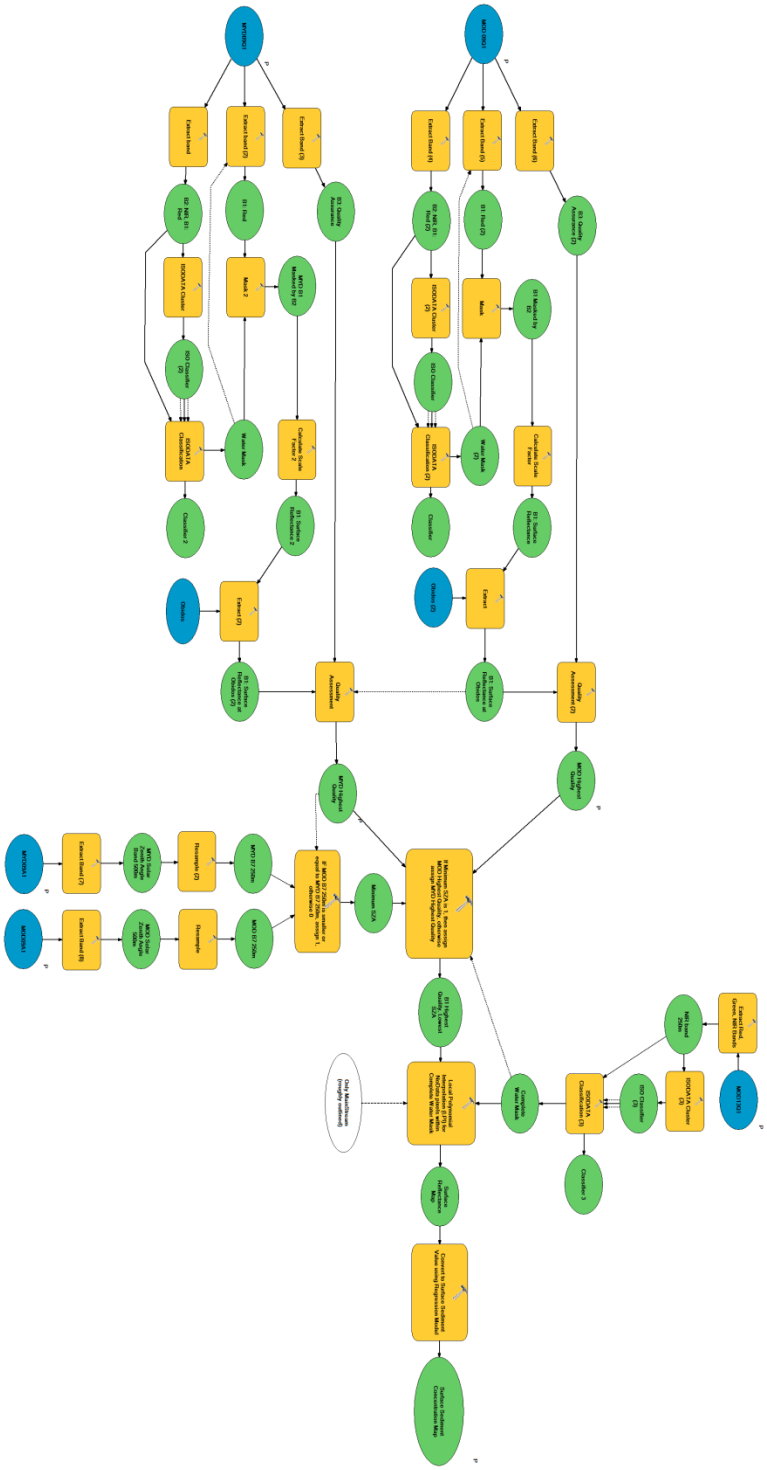

Appendix 2. Script for applying water mask and changing MODIS imagery file name to YYYYMMDD format.

```
import arcpy, os, time, datetime
from arcpy import env
env.workspace = r"C:\Users\scv\Desktop\test2"
env.overwriteOutput = True
arcpy.CheckOutExtension("spatial")

try:
	SSCmap_List = os.listdir(r"path1")
	WaterExtent_List = os.listdir(r"path2")
	for SSCmaps in SSCmap_List:
		for WaterExtent in WaterExtent_List:
			if int(SSCmaps[13:16]) < int(WaterExtent[13:16])+16 and int(SSCmaps[13:16]) >=
int(WaterExtent[13:16]):
				Extracted_SSCmaps = arcpy.sa.ExtractByMask(SSCmaps, WaterExtent)
				Extracted_SSCmaps.save(r"\Extracted_{0}".format(SSCmaps))
except:
	pass # pass for now

Raster_list = arcpy.ListRasters("", "tif")
for files in Raster_list:
	julian = files[9:16]
	a = datetime.datetime.strptime(julian, "%Y%j")
	yyyymmdd = a.strftime("%Y%m%d")
	new_name = yyyymmdd + files

	arcpy.Copy_management(files, r"\subfolder\{0}".format(new_name))
	print new_name + " " + arcpy.GetMessage(arcpy.GetMessageCount() -1)
```

Appendix 3. Figure 4 in Kilham et al., 2011

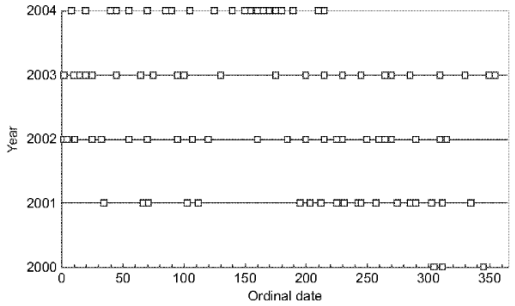

Figure 4. Data availability for MOD09A1 (8-day composite, Terra) images for the central Amazon Basin. Ordinal date on *x*-axis compared to highest quality images (rated 3 or 4, see text) for h11v09 and h12v09 for years 2000–2004 indicated by the *y*-axis position. On average approximately 20 images were available per year. Most notably, a significant number of images are available for early in the season of rising water starting December through March.

REFERENCES

Albanakis, K. S. (1990) Testing of a model for the simulation of the volume reflectance of water due to suspended sediment under controlled conditions, for various sediment types. *International Journal of Remote Sensing,* 11, 1533-1547.

ANEEL. (1999) *The state of water in Brazil.* The National Electric Energy Agency, Brasilia, Brazil.

Baker, E. T and W. J. Lavelle (1984) The effect of particle size on the light attenuation coefficient of natural suspensions. *Journal of Geophysical Research,* 89, 8197–8203.

Bhargava, D. S and D. W. Mariam (1991) Effects of suspended particle size and concentration on reflectance measurements. *Photogrammetric Engineering and Remote Sensing,* 57, 519–529.

Bi. N, Z. Yang, H. Wang, D. Fan, X. Sun and K. Lei (2011) Seasonal variation of suspended-sediment transport through the southern Bohai Strait. *Estuarine, Coastal and Shelf Science,* 93, 239-247.

Binding, C. E., D. G. Bowers and E. G. Mitchelson-Jacob (2005) Estimating suspended sediment concentrations from ocean colour measurements in turbid waters: the impact of variable particle scattering properties. *Remote Sensing of Environment,* 94, 373-383.

Birkett, C., L. A. K. Mertes, T. Dunne, M. H. Cost and M. J. Jasinski (2002) Surface water dynamics in the Amazon Basin: application of satellite radar altimetry. *Journal of Geophysical Research-Atmospheres,* 107, 21.

Bonnet, M. P., G. Barroux, J. M. Martinez, F. Seyler, P. Moreira-Turcq, G. Cochonneau, J. M. Melack, G. Boaventura, L. Maurice-Bourgoin, J. G. Leon, S. Calmant, P. Kosuth, J. L. Guyot and P. Seyler (2008) Floodplain hydrology in an Amazon floodplain lake (Lago Grande de Curuai). *Journal of Hydrology,* 349, 18-30.

Bourgoin, L. M, M. Bonnet, J. Martinez, P. Kosuth, G. Cochonneau, P. Moreira-Turcq, J. L. Guyot, P. Vauchel, N. Filizola and P. Seyler (2007) *Journal of Hydrology,* 335, 140-156.

Curran, P. J. and E. M. M. Novo (1988) The relationship between suspended sediment concentration and remotely sensed spectral radiance: a review. *Journal of Coastal Research,* 4, pp. 351–368.

Dunne, T., L. A. K. Mertes, R. H. Meade, J. E. Richey and B. R. Forsberg (1998) Exchanges of sediment between the flood plain and channel of the Amazon River in Brazil. *Geological Society of America Bulletin,* 110**,** 450-467.

Filizola, N. (1999) O fluxo de seimentos em suspense o nos rios da bacia Amazonica Brasileira. ANEEL, Brasilia, 63.

Filizola, N. and J. L. Guyot (2004) The use of Doppler technology for suspended sediment discharge determination in the River Amazon. *Hydrological Sciences Journal,* 49**,** 143-153.

Filizola, N., F. Seyler, M. H. Mourao, W. Arruda, N. Spinola and J. L. Guyot (2009) STUDY OF THE VARIABILITY IN SUSPENDED SEDIMENT DISCHARGE

AT MANACAPURU, AMAZON RIVER, BRAZIL. *LATIN AMERICAN JOURNAL OF SEDIMENTOLOGY AND BASIN ANALYSIS,* 16**,** 93-99.

Filizola, N., J. L. Guyot, H. Wittmann, J. M. Martinez, and E. Oliveira (2011) The Significance of Suspended Sediment Transport Determination on the Amazonian Hydrological Scenario, In *Sediment Transport in Aquatic Environments (ed Manning, A. J.*), InTech, 45-64.

Forget, F., S. Ouillon, F. Lahet, P. Broche (1999) Inversion of reflectance spectra of nonchlorophyllous turbid coastal waters. Remote Sensing of Environment, 68, 264-272.

Galvão, L. S., J. R. dos Santos, D. A. Roberts, F. M. Breunig, M. Toomey and Y. M. de Moura (2011) On intra-annual EVI variability in the dry season of tropical forest: A case study with MODIS and hyperspectral data. *Remote Sensing of Environment*, 115**,** 2350-2359

Hess, L. L., J. M. Melack, E. M. L. M. Novo, C. C. F. Barbosa and M. Gastill (2003) Dual-season mapping of wetland inundation and vegetation for the central Amazon basin. *Remote Sensing of Environment*, 87, 404-428.

Hu, C., Z. Chen, T. D. Clayton, P. Swarzenski, J. C. Brock and F. E. Muller–Karger (2004) Assessment of estuarine water-quality indicators using MODIS medium-resolution bands: Initial results from Tampa Bay, FL. *Remote Sensing of Environment*, 93**,** 423-441.

Kilham, N. and D. Roberts (2011) Amazon River time series of surface sediment concentration from MODIS. *International Journal of Remote Sensing,* 32**,** 2659-2679.

Kirk, J. T. O. (1989) The upwelling light stream in natural waters. *Liminology and Oceanography,* 34**,** 1410-1425.

Latrubesse, E. M. and E. Franzinelli (2002) The Holocene alluvial plain of the middle Amazon River, Brazil. *Geomorphology*, 44, 241-257.

Latrubesse, E. M. and E. Franzinelli (2005) The late Quaternary evolution of the Negro River, Amazon, Brazil: Implication for island and floodplain formation in large anabranching tropical systems. *Geomorphology*, 70, 372-397.

Latrubesse, E. M., J. C. Stevaux and R. Sinha (2005) Tropical rivers. *Geomorphology*, 70**,** 187-206.

Latrubesse, E. M. (2008) Patterns of anabranching channels: The ultimate end-member adjustment of mega-rivers. *Geomorphology*, 101, 130-145.

Latrubesse, E. M., M. Cozzuol, S. A. F. Silva-Caminha, C. A. Rigsby, M. L. Absy and C. Jaramillo (2010) The Late Miocene paleogeography of the Amazon Basin and the evolution of the Amazon River system. *Earth Science Reviews*, 99, 99-124.

Latrubesse, E. M. (2012) Amazon Lakes, In *Lakes and Reservoirs (ed Bengtsson, L., R. Herschy and R. Fairbridge)*, Springer Verlag, 13-26.

Li, W. H., R. Weeks and A. R. Gillespie (1998) Multiple scattering in the remote sensing of natural surfaces. *International Journal of Remote Sensing,* 19**,** 1725-1740.

Martinelli, L. A., B. R. Forsberg, R. L. Victoria, A. H. Devol, J. R. Mortatti, J. Ferreira, J. Bonassi and E. Oliveria (1993) Suspended sediment load in the Madeira

river.*Mitteilungen aus dem Geologisch-Palaonologischen* Institut der Universitat Hamburg 74, 41-54.

Martinez, J. M., L. M. Bourgoin, P. Kosuth, F. Seyler and J. L. Guyot (2003) Analysis of multitemporal MODIS and Landsat 7 images acquired over Amazonian floodplains lakes for suspended sediment concentrations retrieval. *IEEE***,** 2122-2124.

Martinez, J. M., J. L. Guyot, N. Filizola and F. Sondag (2009) Increase in suspended sediment discharge of the Amazon River assessed by monitoring network and satellite data. *Catena,* 79**,** 257-264.

Meade, R. H (1994) Suspended sediments of the modern Amazon and Orinoco Rivers. *Quaternary International*, 21, 29–39.

Mertes, L. A. K., M. O. Smith and J. B. Adams (1993) Estimating Suspended Sediment Concentrations in Surface Waters of the Amazon River Wetlands from Landsat Images. *Remote Sensing of Environment,* 43**,** 281-301.

Mertes, L. A. K. (1994) Rates of flood-plain sedimentation on the central Amazon River. *Geology*, 22, 171-174

Mertes, L. A. K., D. L. Daniel, J. M. Melack, B. Nelson, L. A. Martinelli and B. R. Forsberg (1995) Spatial patterns of hydrology, geomorphology, and vegetation on the floodplain of the Amazon River in Brazil from a remote sensing perspective. *Geomorphology*, 13**,** 215-232.

Mertes, L. A. K., T. Dunne and L. A. Martinelli (1996) Channel-floodplain geomorphology along the Solimoes-Amazon River, Brazil. *Geological Society of America Bulletin,* 108**,** 1089-1107.

Mertes, L. A. K and Magadzire, T. T. (2008) Large Rivers from Space, in *Large Rivers: Geomorphology and Management (ed Gupta A.)*, John Wiley & Sons, Ltd, Chichester, UK.

Miliman, J. D. and R. H. Maede (1983) World-Wide Delivery of River Sediment to the Oceans. *The Journal of Geology,* 91**,** 1-21.

Miller, R. L. and J. F. Cruise (1995) Effects of Suspended Sediments on Coral Growth - Evidence from Remote-Sensing and Hydrologic Modeling. *Remote Sensing of Environment,* 53**,** 177-187.

Miller, R. L. and B. A. McKee (2004) Using MODIS Terra 250 m imagery to map concentrations of total suspended matter in coastal waters. *Remote Sensing of Environment*, 93**,** 259-266.

Min, J., J. Ryu, S. Lee and S. Son (2012) Monitoring of suspended sediment variation using Landsat and MODIS in the Saemangeum coastal area of Korea. *Marine Pollution Bulletin,* 64, 382-390.

Oosterbaan, R. J. (2009) *SegReg: segmented linear regression with breakpoint and confidence intervals*. Available from: http://www.waterlog.info/segreg.htm

Rodríguez-Guzmán, V. and F. Gilbes-Santaella (2009) Using MODIS 250 m Imagery to Estimate Total Suspended Sediment in a Tropical Open Bay. *INTERNATIONAL JOURNAL OF SYSTEMS APPLICATIONS, ENGINEERING & DEVELOPMENT*, 3.

Richey, J. E., R. H. Meade, E. Salati, A. H. Devol, C. F. Nordin and U. Dossantos (1986) Water discharge and suspended sediment concentrations in the Amazon River 1982–1984. *Water Resources Research*, 22, 756–764.

Sipelgas, L., U. Raudsepp, T. and Kouts (2006) Operational monitoring of suspended matter distribution using MODIS images and numerical modeling. *Advances in Space Research*, 38, 2182-2188.

Sippel, S. J., S. K. Hamilton and J. M. Melack (1992) Inundation area and morphometry of lakes on the Amazon River floodplain, Brazil. *Archive for Hydrobiology,* 123, 385-400.

Stumpf, R. P. and P. M. Goldschmidt (1992) Remote Sensing of Suspended Sediment Discharge into the Western Gulf of Maine during theApril 1987 100-Year Flood. *Journal of Coastal Research,* 8**,** 218-225.

Tassan, S. (1994) Local Algorithms Using Seawifs Data for the Retrieval of Phytoplankton, Pigments, Suspended Sediment, and Yellow Substance in Coastal Waters. *Applied Optics,* 33**,** 2369-2378.

UNEP GEMS/WATER (1994) *Global Environemnt Monitorng System – Water Program.* National Water Research Institute, Burlington, Canada.

Vermote, E. F. and A. Vermeulen (1999) *ATMOSPHERIC CORRECTION ALGORITHM: SPECTRAL REFLECTANCES (MOD09)* (NASA contract NAS5-96062). Department of Geography, College Park, Maryland, USA.

Vermote, E. F., S. Y. Kotchenova and J. P. Ray (2011). 250 m level 3 surface reflectance band quality description (Table 14), In *MODIS Surface Reflectance User's Guide.* MODIS Land Surface Reflectance Science Computing Facility, College Park, Maryland, USA.

Villar, E., J. M. Martinez, M. Le Texier, J. L. Guyot, P. Fraizy, P. R. Meneses and E. Oliveira (2012) A study of sediment transport in the Madeira River, Brazil, using MODIS remote-sensing images. *Journal of South American Earth Sciences*.

Wang, J., X. Lu. (2010) Estimation of suspended sediment concentration using Terra MODIS: An example from the Lower Yangtze River, China. *Science of the Total Environment*, 408, 1131-1138.

White, H. (1980) A heteroskedasticity-consistent covariance matrix estimator and a direct test for heteroskedasticity. *Econometrica,* 48, 817-838.

Witte, K. H. and W. Heinlein (1981) About the Spectral Dependence of the Refractive-Index Profile of Optical Fibers Given a Linear Relationship between Refractive-Index and Doping Level. *Frequenz,* 35**,** 123-127.

Zhang, M., J. Tang, Q. Dong, Q. Song and J. Ding (2010) Retrieval of total suspended matter concentration in the Yellow and East China Seas from MODIS imagery. *Remote Sensing of Environment,* 114, 392-403.